Journal of Orthopaedic Translation 33 (2022) 90–106

Contents lists available at ScienceDirect

Journal of Orthopaedic Translation

journal homepage: www.journals.elsevier.com/journal-of-orthopaedic-translation

3D printed porous sulfonated polyetheretherketone scaffold for cartilage repair: Potential and limitation

Zhiguo Yuan [a,1], Teng Long [a,1], Jue Zhang [a,1], Zhuocheng Lyu [a], Wei Zhang [a], Xiangchao Meng [a], Jin Qi [b], You Wang [a,*]

[a] Department of Bone and Joint Surgery, Department of Orthopaedics, Renji Hospital, School of Medicine, Shanghai Jiaotong University, Shanghai, China
[b] Shanghai Institute of Traumatology and Orthopaedics, Ruijin Hospital, School of Medicine, Shanghai Jiao Tong University, Shanghai, China

ARTICLE INFO

Keywords:
3D printing
Polyetheretherketone(PEEK)
Focal cartilage defects
Cartilage tissue engineering scaffold
In vivo study

ABSTRACT

Objective: The treatment of cartilage lesions has always been a difficult problem. Although cartilage tissue engineering provides alternative treatment options for cartilage lesions, biodegradable tissue engineering scaffolds have limitations.

Methods: In this study, we constructed a porous PEEK scaffold via 3D printing, surface-engineered with concentrated sulfuric acid for 15 s (SPK-15), 30 s (SPK-30), and 60 s (SPK-60). We systematically evaluated the physical and chemical characteristics and biofunctionalities of the scaffolds, and then evaluated the macrophage polarization modulating ability and anti-inflammatory effects of the sulfonated PEEK, and observed the cartilage-protective effect of SPK using a co-culture study. We further evaluated the repair effect of PEEK and SPK by implanting the prosthetic scaffold into a cartilage defect in a rabbit model.

Results: Compared to the PEEK, SPK-15 and SPK-60 scaffolds, SPK-30 has a good micro/nanostructure, appropriate biomechanical properties (compressive modulus, 43 ± 5 MPa; Shaw hardness, 20.6 ± 1.3 HD; close to native cartilage, 30 ± 8 MPa, 17.8 ± 0.8 HD), and superior biofunctionalities. Compared to PEEK, sulfonated PEEK can favor macrophage polarization to the M2 phenotype, which increases anti-inflammatory cytokine secretion. Furthermore, SPK can also prevent macrophage-induced cartilage degeneration. The in-vivo animal experiment demonstrates that SPK can favor new tissue ingrowth and integration, prevent peri-scaffold cartilage degeneration and patellar cartilage degeneration, inhibit inflammatory cytokine secretion, and promote cartilage function restoration.

Conclusion: The present study confirmed that the 3D printed porous sulfonated PEEK scaffold could promote cartilage functional repair, and suggests a new promising strategy for treating cartilage defects with a functional prosthesis that spontaneously inhibits nearby cartilage degeneration.

Translational potential of this article: In the present study, we propose a new cartilage repair strategy based on a porous, non-biodegradable polyetheretherketone (PEEK) scaffold, which may bring up a new treatment route for elderly patients with cartilage lesions in the future.

1. Introduction

Articular cartilage is an avascular connective tissue that can transmit forces to the subchondral bone [1]. The avascular nature of cartilage contributes to its poor capacity for self-repair upon trauma or disease, and even focal cartilage defects (FCDs) can lead to osteoarthritis (OA) if left untreated [2]. Current clinical treatments for FCDs include cartilage transplantation [3,4], mosaicplasty [5], microfracture [6], and autologous chondrocyte implantation (ACI) [7]. Although these strategies can provide transitory pain relief and recover joint mobility, none of these strategies can fully restore the structure and function of the articular cartilage [8].

Tissue engineering may provide alternative treatments for FCDs and subsequent cartilage degeneration in OA [9]. Although tissue engineering can provide alternative treatment options, it remains challenging to rapidly reconstruct the compositional, structural, and functional changes

* Corresponding author.
E-mail address: drwangyou@126.com (Y. Wang).
[1] these authors contributed equally to the work.

https://doi.org/10.1016/j.jot.2022.02.005
Received 17 November 2021; Received in revised form 8 February 2022; Accepted 14 February 2022

of cartilage in a short time for adult patients, especially in elderly patients [10]. Besides the complexity of clinically applying seeding cells, a bottleneck results from biodegradable scaffolds; there are requirements for these scaffolds to have appropriate physical structures and chemical characteristics, as well as obtaining permission for their clinical application as a product of a "medical device," are quite complicated.

Ideally engineered cartilage scaffolds should fulfill the following requirements: 1) superior biocompatibility; 2) excellent porous and interconnected architecture with open porosity to facilitate cell migration, nutrient flow, and tissue formation; 3) biodegradability with a suitable degradation rate matched with tissue regeneration; and 4) good biomechanical properties and consistency during the tissue regeneration process [11].

For a typical cartilage scaffold, there are three major challenges for cartilage regeneration and functional replacement: one is to achieve the initial biomechanical strength of the scaffold with the native tissue; the second is to maintain the degradation rate consistent with the tissue regeneration speed; and the third is to maintain the biomechanical functions during the process of scaffold degradation and tissue growth. Furthermore, these three characteristics are difficult to achieve using traditional tissue engineering scaffolds. For example, the mechanical strength of natural biomaterials (collagen [12], alginate [13], chitosan [14], gelatin [15], and silk [16]) are mismatched with those of native cartilage. Compared to natural biomaterials, some synthetic materials (such as polylactic acid (PLA) [17], polylactide-co-glycolide (PLGA) [18], and polycaprolactone (PCL) [19]) have ideal mechanical properties. However, their poor cell attachment, tendency to produce acidic products during degradation, and unstable mechanical properties during degradation and tissue regeneration present a critical hurdle for their clinical application [20].

To address the above challenges, we propose a new cartilage tissue engineering approach for chondral functional repair based on a non-biodegradable scaffold. We aim to design a novel nondegradable, high-strength, porous scaffold that can provide appropriate biomechanical support in the early stage of chondral repair, and eventually coexist with ingrowth of the new tissue. Compared to traditional degradable scaffolds, the new non-biodegradable scaffold has two main advantages: it can avoid the disadvantage of unstable biomechanical function of scaffolds during degradation, and it can compensate for the reduction of the opportunity for cartilage regeneration for elderly patients as a porous prosthesis.

High-performance poly (ether ketone) (PEEK) has gained wide interest as an orthopedic implant in the medical field [21]. It is a promising material for implantation because it is highly strong and suitable for high load-bearing applications. In our previous study, we fabricated a new PEEK implant for treating local osteochondral defects and demonstrated that the PEEK implant had a better cartilage protection effect than the metal implant. However, the modulus of block-shaped PEEK is 3–4 GPa [22], while the modulus of native cartilage is approximately 25 MPa [23]. The modulus mismatch between PEEK and cartilage can lead to cartilage degeneration. Moreover, several previous studies have shown that implant mechanical properties may result in cartilage degeneration, mainly because of its mismatched modulus [24,25]. For example, Custers et al. treated cartilage defects with OxZr and CoCr implants in a goat model and revealed that cartilage degeneration could not be prevented by metal implants at a one-year follow-up [26]. To the best of our knowledge, the compressive modulus of porous materials is much lower than that of block-shaped materials. To match the compressive modulus of the PEEK scaffold with normal native cartilage, three-dimensional (3D) printed PEEK porous scaffolds were manufactured via fused filament fabrication (FFF).

As it is a material that is chemically and biologically inert, the biocompatibility and bioactivity of PEEK should be enhanced [27]. In recent years, sulfonation has become an effective approach for surface modification to fabricate micro- and nanostructures on the surface of PEEK, which can modify its surface mechanical properties and is beneficial for cell attachment and proliferation [28,29]. In this study, we constructed a porous PEEK scaffold using 3D printed technologies and fabricated a porous 3D network on the surface using concentrated sulfuric acid. We systematically evaluated the physical and chemical characteristics and biofunctionalities of sulfonated PEEK (SPK) with a nanostructured network. We also investigated the feasibility and safety of the SPK scaffold used for cartilage repair in a focal chondral defect model.

2. Materials and methods

2.1. Scaffold preparation

These PEEK scaffolds were additively manufactured via a 3D printer (Funmat, Intamsys Technology, Shanghai, China) using a PEEK filament (450G, Victrex, Lancashire, UK). For cell ingrowth and proliferation, the pore structures of the constructs should be considered. The pore size was designed to be 500 μm with a 250-μm strut size in this study, based on some previous studies [30–32], which confirmed that the ideal pore size for tissue ingrowth should be between 250 and 500 μm. The printing parameters, layer height, temperature, and printing speed, were designed to establish a set of consistent parameters (Table 1). Samples used for characterization analysis and cell seeding were Ø6 mm × 1 mm cylinders, samples for biomechanical testing were Ø4 mm × 3 mm cylinders, and samples for in vivo experiments were Ø4 mm × 1 mm cylinders.

To acquire a uniform porous surface, ultrasonic and magnetic stirring were used in the sulfonation treatment. These 3D printed PEEK scaffolds were immersed in concentrated sulfuric acid solution (98 wt%) and subjected to ultrasonic oscillation for 15 s, 30s, and 60 s. Then, the scaffolds were washed with distilled water at 120 °C and stirred for 6 h. The unsulfonated sample was designated PEEK, whereas SPK-15, SPK-30, and SPK-60 denote the samples treated with sulfuric acid at room temperature for 15s, 30s, and 60 s, respectively.

2.2. Physiochemical characteristics of scaffolds

2.2.1. Chemical and morphological characterization of scaffolds

The surface morphology and elemental composition of PEEK, SPK-15, SPK-30, and SPK-60 scaffolds were determined by scanning electron microscopy (SEM) (Hitachi S-4800, Hitachi, Tokyo, Japan) and energy-dispersive X-ray spectrometry (EDS) (Hitachi S-4800, Hitachi, Tokyo, Japan). The functional groups of PEEK, SPK-15, SPK-30, and SPK-60 were identified by Fourier transform infrared spectrometry (FTIR, Magna-IR 750, Nicolet, Thermo Fisher Scientific), and the spectra were recorded from 650 cm^{-1} to 4000 cm^{-1}. The crystalline phases of these scaffolds were examined by XRD (Shimadzu, Kyoto, Japan), and XRD analysis was performed using a D8 ADVANCE X-ray diffractometer (Bruker, Germany) in a 2 theta range of 10–80° with Cu Kα radiation. The elemental constituents of these samples, PEEK, SPK-15, SPK-30, and SPK-60, were identified using X-ray photoelectron spectroscopy (XPS, AXIS Ultra, Kratos Analytical Ltd, Kyoto, Japan). These samples charging was referenced to the C 1s line at 285.0 eV, and deconvolution of the S2p spectra was performed using the least-squares peak analysis software XPS PEAK95 Version 3.1 and the Lorenzian-Gaussian peak fitting model.

The surface morphology of these samples, PEEK, SPK-15, SPK-30, and SPK-60, were characterized using a 3D confocal laser microscopy (Shape measurement laser microscope, Keyence, VK-X 100, Osaka, Japan). The roughness of the line of PEEK, SPK-15, SPK-30, and SPK-60 scaffolds were determined by the average roughness (Ra) values. The surface areas of PEEK, SPK-15, SPK-30, and SPK-60 were determined by N_2

Table 1
Final printing parameters used for printing porous PEEK.

Nozzle Size	Layer Height	Nozzle Temperature	Printing Speed
0.25 mm	0.25 mm	420–450 °C	2200 mm/min

adsorption–desorption isotherms obtained at 77 K with a Micromeritics ASAP-2020, based on the BET method. The porosity and pore size distribution measurements of PEEK, SPK-15, SPK-30, and SPK-60 were determined using mercury porosimetry (Micromeritics AutoPore IV 9500).

2.2.2. Biomechanical characteristics of scaffolds

The scaffolds used for biomechanical testing were fabricated in a consistent cylindrical form of Ø4 mm × 3 mm. Uniaxial compressive tests were performed at a rate of 1 mm/min using a mechanical tester (Instron, model 5969, High Wycombe, UK) at room temperature. The compressive modulus of PEEK, SPK-15, SPK-30, and SPK-60 scaffolds were computed via the stress–strain curve, and five duplicate specimens were tested for each case. The hardness of PEEK, SPK-15, SPK-30, and SPK-60 scaffolds were determined using a Shore hardness tester (Haibao Measuring Instrument, Zhejiang, China).

Nanoindenter experiments were carried out using a Hysitron-TI 950 TriboIndenter at room temperature. A minimum of 15 points were chosen and measured for each sample (n = 5) to evaluate the compressive modulus and hardness. The hardness and compressive modulus of the different surfaces were analyzed by the nanoindentation test, which was performed in depth control mode (100 nm) at a constant rate of 10 nm/s and dwell at a peak depth of 10 s.

As a control group, native cartilage samples used for compressive test, hardness test and nanoindentation test, were obtained from patients who underwent arthroplasty.

2.3. Protein adsorption of scaffolds

Bovine serum albumin (BSA) was used to observe the capacity of adsorbing proteins from different scaffolds: PEEK, SPK-15, SPK-30, and SPK-60 scaffolds. Four different scaffolds were immersed in 1 mL of 0.5 mg/mL BSA (Beijing Solarbio Science & Technology Co, Ltd, Beijing, China) solution in a 48-well cell culture plate for 1, 5, 10, 30, 60, 90, and 120 min. The scaffolds were washed with PBS for 3 min to remove the unadsorbed proteins. To detach BSA from the sample surface, sodium dodecyl sulfate (SDS; 2 wt%) in phosphate-buffered saline (PBS) was used to increase these samples to collect the eluate. The concentration of BSA in the eluate was determined using a BCA protein analysis kit (BCA protein assay kit, Thermo Fisher Scientific). The adsorbed protein content was determined by measuring the absorbance at 562 nm using a microplate reader (Varioskan Flash, Thermo Fisher Scientific), and the final results were characterized by the mass of BSA (mg/scaffold) adsorbed by each scaffold.

To intuitively observe the ability of scaffolds to adsorb protein. PEEK, SPK-15, SPK-30, and SPK-60 scaffolds were placed in BSA-FITC solution (0.5 mg/mL, Beijing Solarbio Science & Technology Co, Ltd.) for 5 min. After washing with PBS, the scaffolds were examined by confocal microscopy (Olympus FLUOVIEW FV3000, Olympus, Japan).

2.4. Cytocompatibility of samples

2.4.1. Chondrocyte isolation and culture

The primary culture of rabbit chondrocytes was carried out as follows: rabbit articular cartilage was dissected from the femoral condyle and patellar groove and sliced into 1 × 1 × 1 mm pieces, which were then digested for 6 h using 0.15% (w/v) collagenase in Dulbecco's modified Eagle's medium (DMEM, Corning, Glendale, AZ, USA) at 37 °C and 5% CO_2. Then, these cells were obtained via centrifugation and cultured in DMEM with 10% (v/v) fetal bovine serum (FBS, HyClone). The cells were diluted (1:3) after 90% confluence was reached. Passage 3 chondrocytes were used for cytocompatibility analysis of the samples.

2.4.2. Cell viability

We utilized chondrocytes to examine the cytotoxicity of these scaffolds after seeding cells on different scaffolds for 3 days. The viability of cells on different scaffolds was measured by live/dead staining. The cell-scaffold constructs were incubated in DMEM containing 0.05% (v/v) calcein-AM and 0.2% (v/v) propidium iodide (PI) at 37 °C for 30 min using a Live/Dead Cell Viability Assay kit (C2015M, Beyotime, Shanghai, China). The constructs were washed with PBS and imaged using a fluorescence confocal microscope (Leica TCS-SP8, Leica Microsystems, Heidelberg, Germany), and the images were analyzed with Imaris software (Bitplane, Zurich, Switzerland).

2.4.3. Cell attachment

Each scaffold was seeded with 1×10^5 chondrocytes in 100 μL of medium in a 96-well cell culture plate. After culturing for 6, 12, 24, and 48 h, the samples were washed with PBS solution three times. The chondrocytes on the scaffolds were counted using a Cell Counting Kit-8, and the OD values of the cells on the samples were measured at 450 nm using a microplate reader (Synergy HT, Bio-tek Co, USA).

2.4.4. Cell proliferation

Each of these scaffolds, PEEK, SPK-15, SPK-30, and SPK-60, was seeded with 1×10^5 chondrocytes in 100 μL of medium in a 96-well cell culture plate. After culturing for 3, 7, and 14 days, chondrocyte proliferation was analyzed using a CCK-8 assay kit. The cell-scaffold constructs were rinsed with PBS and incubated with cell medium (200 μL) containing CCK-8 solution (20 μL) for 4 h at 37 °C, and then the OD values were measured at 450 nm using a microplate reader (Synergy HT, Bio-tek Co.).

2.4.5. Biochemical assays for collagen I and II, and GAG

Collagen I and II, and glycosaminoglycan (GAG) secretion of chondrocytes on these scaffolds was evaluated via biochemical assays after 3, 7, and 14 days of culture. A Tissue GAG Total Content DMMB Colorimetry kit (GenMed, Shanghai, China) was used to measure the GAG secreted by chondrocytes according to the manufacturer's instructions. The GAG secreted by chondrocytes can be divided into two parts: the GAG in constructs and those in the media. For quantitative analysis of collagen I and II, the rabbit collagen type I ELISA assay kit (H142-1-1, Nanjing Jiancheng, Nanjing, China) and rabbit collagen type II ELISA assay kit (H143-1-1, Nanjing Jiancheng, Nanjing, China) were used according to the manufacturer's protocol. Collagen I and II were also measured in both the constructs and in the media.

2.4.6. Immunofluorescence staining of vinculin on samples

Vinculin secreted by chondrocytes seeded on different scaffolds for 3 days was observed by immunofluorescence staining. The cell-scaffold constructs were fixed for 1 h and permeabilized for 30 min. The vinculin of the chondrocytes was then visualized using a vinculin fluorescence staining kit (GMS10279, GenMed, shanghai, China) according to the manufacturer's instructions and imaged using a fluorescence confocal microscope (Leica TCS-SP8, Leica Microsystems).

2.5. Macrophages polarization modulating effect of scaffolds

2.5.1. Immunofluorescence staining of macrophages on scaffolds

The iNOS (green) and CD206 (red) expression of macrophages (RAW 264.7 cells) on different scaffolds, PEEK, SPK-15, SPK-30, and SPK-60, were evaluated by fluorescence staining. After incubation for 4 days, RAW 264.7 cells were obtained and reattached. Then, 4% paraformaldehyde was used to fix the cells, and 0.1% Triton-X was used to permeabilize the cells for 30 min. BSA (1%) was used to block for 1 h. The cells were then incubated with primary antibodies against iNOS (ab210823, 1:50, Abcam) and CD206 (ab64693, 1:50, Abcam) overnight at 4 °C. Subsequently, the sheep anti-rabbit Alexa Fluor 488 (1:100, Abcam) and sheep anti-mouse Alexa Fluor 594 (1:200, Abcam) were combined with the primary antibody for 1 h. Finally, the nuclei were stained with 4',6-diamidino-2-phenylindole (DAPI). Images were

acquired using a fluorescence microscope (Leica TCS-SP8, Leica Microsystems).

2.5.2. RT-PCR

The macrophage polarization-related genes (CCR7, IL-1, iNOS, and CD206) expression of RAW 264.7 cells treated with different scaffolds were determined by RT-PCR. Total RNA was extracted using TRIzol reagent (Invitrogen, Waltham, MA, USA) after the RAW 264.7 cells were cultured on PEEK and SPK for 1 and 4 days. Complementary DNA (cDNA) was reverse-transcribed using a ReverTra Ace kit (Toyobo, Osaka, Japan). Quantitative gene analysis was performed using real-time PCR on a LightCycler 480 system (Roche Applied Science, Indianapolis, IN, USA). The housekeeping gene, β-actin, was used as a reference gene, and the mRNA levels of CCR7, CD206, L-1β, and iNOS were all normalized to the value of the housekeeping gene β-actin. The forward and reverse primers for the genes used in this section are shown in Table 2.

2.5.3. ELISA

The culture medium of RAW 264.7 cells was collected after incubation on PEEK, SPK-15, SPK-30, and SPK-60 for 1 and 4 days. The concentrations of the related cytokines (tumor necrosis factor (TNF)-α, IL-1β, IL-4, and IL-10) in the medium were examined using an enzyme-linked immunosorbent assay (ELISA) kit (Invitrogen) according to the manufacturer's instructions.

2.6. Cartilage degeneration induced by macrophages treated with PEEK and SPK

2.6.1. Co-culture of chondrocytes pellets and macrophages treated with PEEK and SPK

Chondrocytes (1×10^6) were centrifuged at 150×*g* for 5 min, and then incubated for 1 d to obtain pellets. Chondrocyte pellets were placed in the upper wells of a transwell plate (Corning, USA). The PEEK and SPK scaffolds seeded with RAW 264.7 cells were presented in the lower well of the Transwell plate, and for the control group, there were no scaffolds or macrophages added to the lower well. The culture medium was α-MEM (Gibco) with 10% fetal bovine serum (Gibco) and changed every 3 days. After 1 week, the chondrocyte pellets were harvested for analysis (Fig. 7D).

2.6.2. Biochemical assays for DNA and GAG of chondrocytes pellets

After culturing for 7 days, the chondrocyte pellets were collected and photographed. The DNA content of these pellets was extracted and quantitatively evaluated using a DNA extraction and quantification kit (TIANamp, Beijing, China). The GAG content of these pellets was measured using the Tissue GAG Total Content DMMB Colorimetry kit (Genmed Scientific Inc.) according to the manufacturer's instructions.

2.6.3. Immunofluorescence staining of chondrocytes pellets

After harvesting, the chondrocyte pellets were fixed, embedded, and sectioned into 5 μm thick slices, and then stained with immunofluorescence staining for aggrecan (ab3778, 1:100, Abcam), MMP 13 (ab231217, 1:100, Abcam), and collagen II (ab34712, 1:100, Abcam), as described above.

Table 2
Primers used in this study.

Gene	Primers Sequence
CD206	Forward: 5'-TACTTGGACGGATAGATGGAGG-3' Reverse: 5'-CATAGAAAGGAATCCACGCAGT-3'
CCR 7	Forward: 5'-GGTGGCTCTCCTTGTCATTTTC-3' Reverse: 5'-AGGTTGAGCAGGTAGGTATCCG-3'
IL-1	Forward: 5′-AGTTGACGGACCCCAAAAG-3′ Reverse: 5′-TTTGAAGCTGGATGCTCTCAT-3′;
iNOS	Forward: 5'-GAGACGCACAGGCAGAGG-3' Reverse: 5'-CAGGCACACGCAATGATGG-3'
β-actin	Forward: 5'-ACCAGTTCGCCATGGATGAC-3' Reverse: 5'-CACACGCAGCTCATTGTAGA-3'

2.7. In vivo animal studies

2.7.1. Surgical procedure

Animal experiments in the present study were approved by the Animal Ethics Committee of our Hospital. In this study, 54 adult New Zealand white rabbits were allocated into three groups: PEEK, SPK, and untreated control groups. The animals were anesthetized with pentobarbital sodium (3.5% w/v, 1 mL/kg), subsequently, an osteochondral defect (4 mm in diameter and 1 mm in depth) was created on the groove of both knees of rabbits using a sterile punch, and the PEEK or SPK scaffold was implanted into the defect, which was also homogenous in all the samples. The control group was not treated (n = 18 for each group). After the operation, all the rabbits were treated with penicillin for 3 days and returned to their cage, and moved freely. The rabbits were euthanized and assessed at 3, 6, and 12 weeks postoperatively.

2.7.2. Macroscopic evaluation

The femoral trochlear and patella were observed and photographed, and the photographs of each group were independently evaluated by two blinded experienced investigators according to the macroscopic scoring system from Goebel et al. [33]. The rating scale is shown in Table 3.

2.7.3. Histological analyses

Tissue integration of the scaffolds was evaluated by hard tissue slicing, followed by staining with toluidine blue (TB). The samples harvested from the predefined locations of the femoral trochlea were embedded in polymethylmethacrylate. The samples were sectioned to a thickness of 100 μm and then polished to a thickness of 20 μm. The slices were stained with TB to evaluate tissue growth. The length of the tissue to the scaffold (TSC), the proportion of new tissue ingrowth to the scaffold

Table 3

Newly developed macroscopic scoring system		
Parameter	Item	Points
Color of the repair tissue	Hyaline or white	0
	Predominantly white (>50%)	1
	Predominantly translucent (>50%)	2
	Translucent	3
	No repair tissue	4
Presence of blood vessels in the repair tissue	No	0
	Less than 25% of the repair tissue	1
	25–50% of the repair tissue	2
	50–75% of the repair tissue	3
	More than 75% of the repair tissue	4
Surface of the repair tissue	Smooth, homogeneous	0
	Smooth, heterogeneou	1
	Fibrillated	2
	Incomplete new repair tissue	3
	No repair tissue	4
Graft level with surrounding cartilage	In level with adjacent cartilage	0
	Raised or Below <25% repair of defect depth	1
	Raised or Below ≥25% < 50% repair of defect depth	2
	Raised or Below≥50% < 75% repair of defect depth	3
	Raised or Below≥75% repair of defect depth	4
Degeneration of adjacent articular cartilage	Normal	0
	Cracks and/or fibrillations in integration zone	1
	Diffuse osteoarthritic changes	2
	Extension of the defect into the adjacent cartilage	3
	Subchondral bone damage	4

The reverse scale consists of five major parameters and 25 items. A total number of 20 points is achieved for the worst possible result.

(NTIS), and the length of the bone to the scaffold (BSC) were determined according to the histological images. The percentages of TSC, NTIS, and BSC were calculated. SEM was used to observe the tissue ingrowth and scaffold integration. EDS was used to observe the interface composition of the scaffolds with the surrounding tissue.

The samples were fixed in 4% paraformaldehyde for 3 days, decalcified in 15% (w/v) ethylenediaminetetraacetic acid (EDTA), embedded in paraffin, and sectioned into slices with an approximate thickness of 5 μm using a paraffin microtome (Leica EG 1160). HE, SO/FG, and Masson's trichrome staining were performed to observe the adjacent cartilage of the scaffolds. The histological sections were observed by two independent investigators and semi-quantitatively evaluated through histological OARSI scoring for adjacent cartilage degeneration of scaffolds for chondral defects. Histological grading scores were generated separately from the cartilage located on the left and right sides of the scaffolds, and the final scores were determined by the average score.

2.7.4. Micro-CT evaluation

Osteochondral repair was evaluated by micro-CT at 3, 6, and 12 weeks postoperatively. After the animals were euthanized, the samples were harvested and fixed in 4% (w/v) buffered paraformaldehyde for 2 days. The femoral condyle of rabbits was subjected to micro-CT analysis using a Micro-CT 50 scanner (Scanco Medical, Brüttisellen, Switzerland) with 43-μm axial slices. After scanning, the 3D models were reconstructed using the Geomagic Studio 10.0 software program (Research Triangle Park, Chapel Hill, NC, USA). The new bone tissue of the repair region was analyzed through BMD, BV/TV, and Tb.N.

2.7.5. Biomechanical analysis of repair tissue

The pull-out test was used to evaluate the bonding interface between

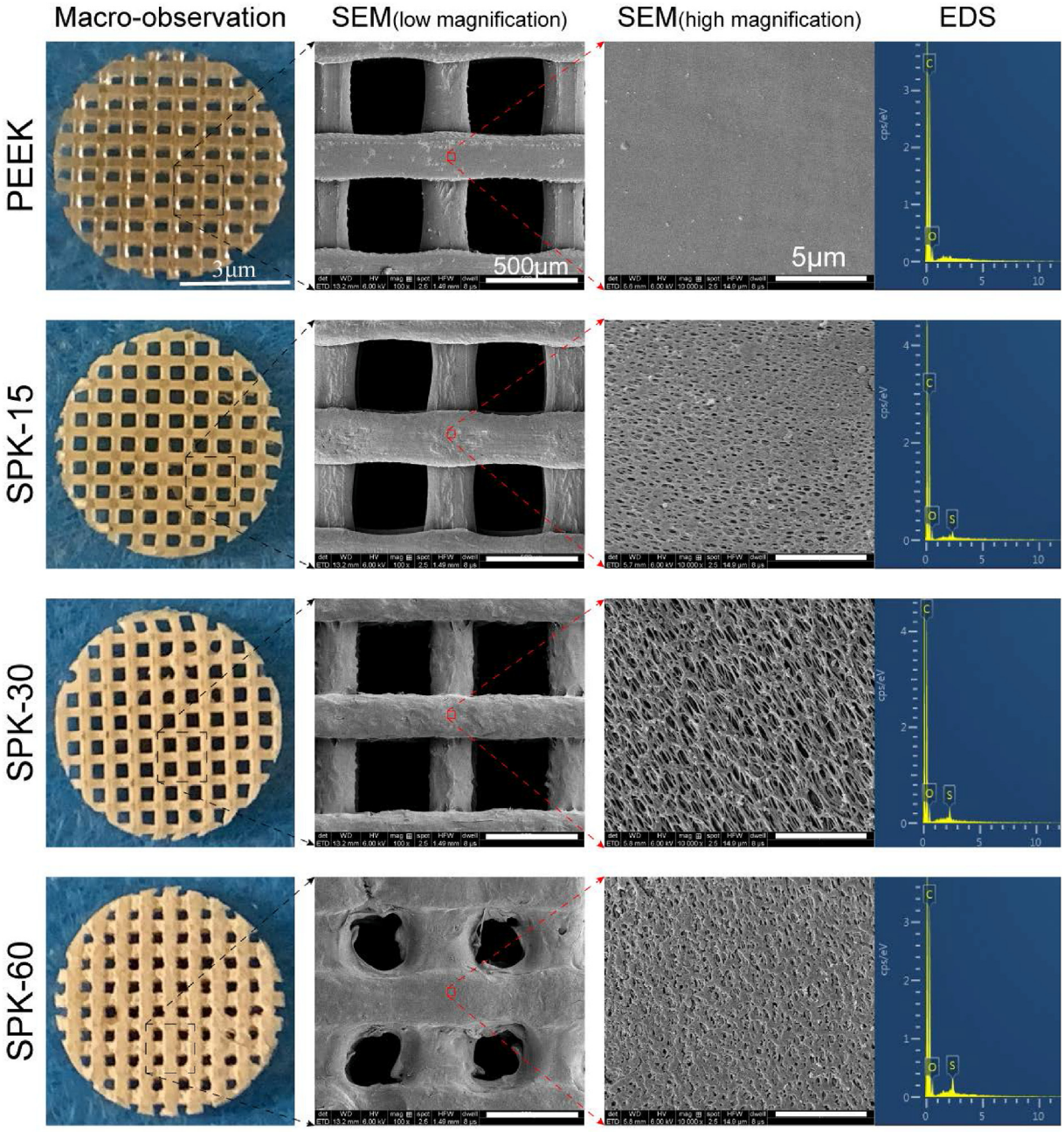

Figure 1. Morphology of various scaffolds (PEEK; SPK-15; SPK-30; SPK-60). The EDS spectra show the elemental composition.

the tissue and the scaffolds. To quantify the load of pulling out the scaffold from the femoral condyle, we used the nylon thread crossed through the scaffold and used a biomechanical machine (model 5969; Instron, High Wycombe, UK) to conduct the pull-out tests (Fig. 11E). The samples were harvested and measured at 3, 6, and 12 weeks post-operatively. The test was performed at a loading rate of 1 mm/min, and the failure load was defined as the maximum load value. The pull-out load was determined by averaging the results from three pull-out tests.

We also used compression tests to investigate the compressive modulus of repair tissue with scaffolds at 3, 6, and 12 weeks post-operatively. The compressive properties were measured using a universal testing machine (model 5969; Instron, High Wycombe, UK) at a compression rate of 0.5 mm min-1 at room temperature. All the samples were prepared in the form of cylinders (Φ4 mm × 3 mm) and vertically placed between two parallel plates. The modulus was computed with the initial slope of the stress–strain curve.

2.8. The chondroprotective effect of scaffolds

The protective effect of the scaffolds was evaluated by macro-observation and histological analysis of the contralateral patellar cartilage. The patella was harvested after rabbit euthanasia at 3, 6, and 12 weeks after surgery. After fixation, decalcification, and embedding, the samples were sectioned into slices. HE, TB, and SO/FG staining were conducted to assess proteoglycans and collagen in the matrix. The histological sections were semi-quantitatively evaluated using the Mankin scoring for the contralateral patellar cartilage.

Furthermore, in order to observe changes in IL-1β and TNF-α in the rabbit knee joint at 3, 6, and 12 weeks post-surgery, the knee joint fluid of rabbits was harvested and tested via ELISA kits (Invitrogen and Thermo Fisher) according to the manufacturer's instructions.

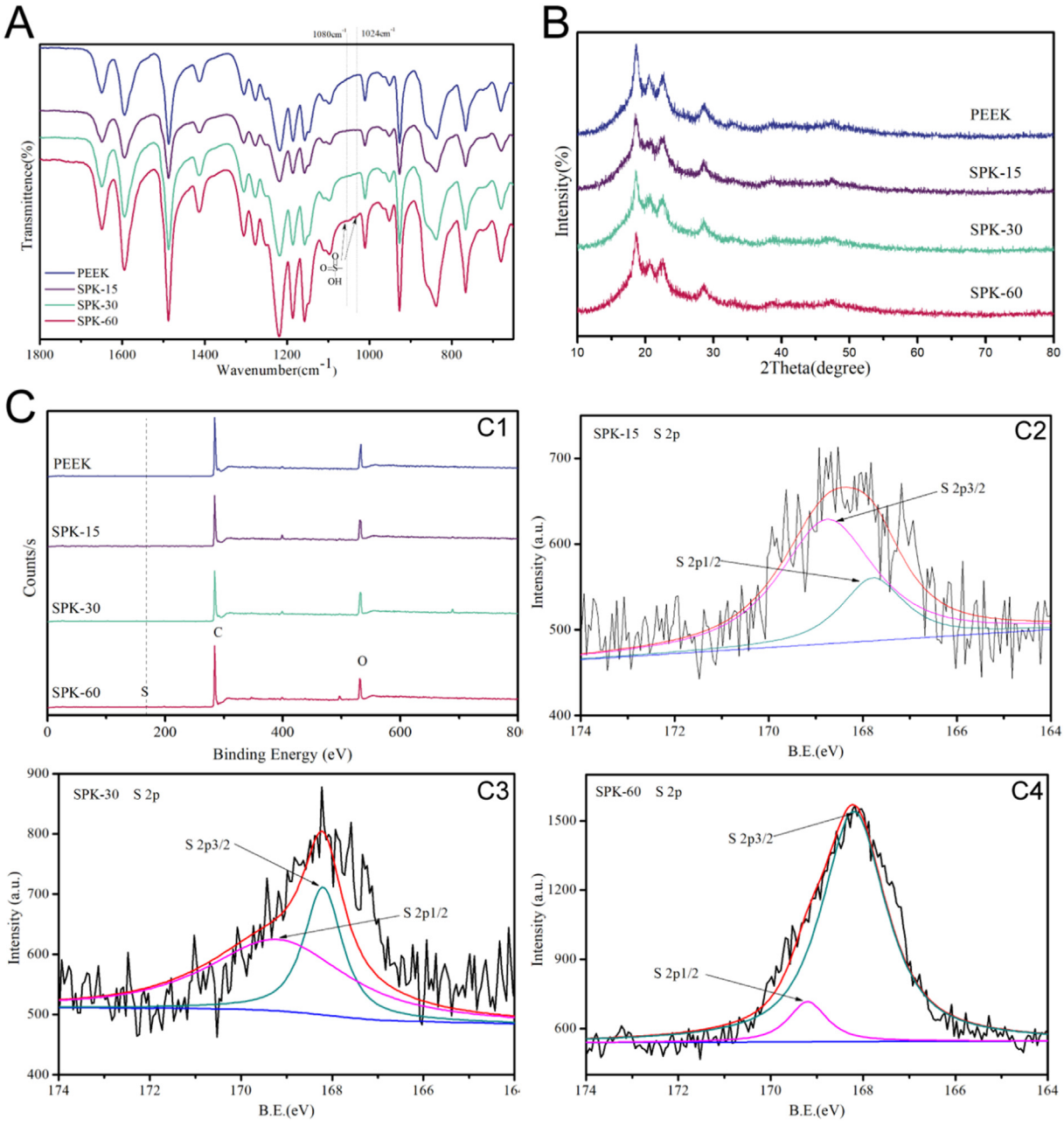

Figure 2. Component analysis of various scaffolds (PEEK; SPK-15; SPK-30; SPK-60). A. FTIR spectra of scaffolds. B. XRD patterns of scaffolds. C. XPS wide scan spectra of PEEK, SPK-15, SPK-30, SPK-60 (C1), and the S 2p core level spectra of SPK-15 (C2), SPK-30 (C3), SPK-60 (C4).

2.9. Statistical analysis

Statistically significant differences were determined using the t-test, one-way analysis of variance (ANOVA) and two-way ANOVA using SPSS 19.0. Data are shown as means ± standard deviation (SD), and the significant difference was set at *P < 0.05, **P < 0.01.

3. Results

3.1. Surface characteristics of scaffolds

The surface microstructure and elemental composition of PEEK, SPK-15, SPK-30, and SPK-60 scaffolds were evaluated by macroscopic observation, SEM, and EDS (Fig. 1). Macroscopically, PEEK, SPK-15, and SPK-30 showed a homogeneous 3D porous structure, whereas the porous structure of SPK-60 was not uniform. Microscopically, the surface of PEEK was smooth with minimal detectable surface features, while a porous micro-nano architectural structure was observed on the surface of the sulfonated PEEK scaffolds. The surface pore structure changed with sulfonation treatment time. For SPK-15, the micropore structure is sparse and discrete. For SPK-30, the surface micropores were homogeneous and interconnected, while for SPK-60, the micropores became smaller and accumulated. The sulfur content varied with the sulfonation treatment time. The EDS spectra confirmed that S existed and varied on the surface of the sulfonated PEEK (Fig. 1).

FT-IR spectra were used to determine the chemical group changes of the different scaffolds and to demonstrate that the characteristic bands were present. These bands include the diphenylketone bands (926, 1490, and 1650 cm^{-1}), diaryl groups (C–O–C stretching at 1158 and 1188 cm^{-1}), and C═C stretching (1600 cm^{-1}). These results also demonstrated that the sulfonated PEEK was similar to PEEK in its main chemical structures. The characteristic polymer bands from sulfonated PEEK confirmed that the SO_3H functional groups were immobilized on the surface of the PEEK scaffold by sulfonation (Fig. 2A).

Moreover, as shown in Fig. 2B, there was no significant difference in the XRD patterns of PEEK, SPK-15, SPK-30, and SPK-60, which all have the characteristic peaks of PEEK.

The surface elemental compositions of PEEK, SPK-15, SPK-30, and SPK-60 from the XPS analysis are shown in Fig. 2C. The elements of C1s and O1s were observed, and the two peaks (168.1 eV, 169.2 eV) were related to the 2p3/2 and 2p1/2 of sulfur (Fig. 2C2, C3, C4). Compared with PEEK substrates, S existed on the surface of sulfonated PEEK, and more sulfur content was immobilized on the PEEK with increasing sulfonation time.

The surface morphologies of the different scaffolds, PEEK, SPK-15, SPK-30, and SPK-60, were observed using an optical profilometer (Fig. 3A). The surface roughness of PEEK, SPK-15, SPK-30, and SPK-60 could be evaluated using the Ra value, which showed that the surface roughness of PEEK increased with the prolongation of sulfonation treatment time, and the differences were significant (P < 0.05) (Fig. 3B).

The surface areas of PEEK, SPK-15, SPK-30, and SPK-60 were measured using the Brunauer–Emmett–Teller (BET) method, and the surface areas of PEEK, SPK-15, SPK-30, and SPK-60 were 1.593 ± 0.038, 1.73 ± 0.04, 2.128 ± 0.169, and 2.282 ± 0.177 m^2/g, respectively (Fig. 3C). Moreover, the BET surface areas of SPK-30 and SPK-60 were higher than those of PEEK and SPK-15 (P < 0.05).

The pore size and porosity of these different samples were determined using mercury porosimetry, and the porosities of PEEK, SPK-15, SPK-30, and SPK-60 were 50.6 ± 2.13, 53.37 ± 0.95, 59.44 ± 0.81, and 59.49 ± 2.79%, respectively. At the micro-scale, the median pore diameters of PEEK, SPK-15, SPK-30, and SPK-60 were 398.9, 401.2, 402.5, and 258.8 μm, respectively, while the median micropore diameters of PEEK, SPK-15, SPK-30, and SPK-60 were 10.3, 750.5, 2100.9, and 800.3 nm at the nanoscale, respectively (Fig. 3D, E, F).

3.2. Biomechanical properties of samples

The integral biomechanical properties of these different scaffolds were evaluated through compression and hardness tests, while the surface biomechanical characteristics of these different scaffolds were determined by nanoindenter experiments. For compression tests, the compressive modulus of these scaffolds was computed using the stress–strain curve, and the results are shown in Fig. 4A. The compressive modulus of SPK-30 was lower than that of PEEK, SPK-15, and SPK-60,

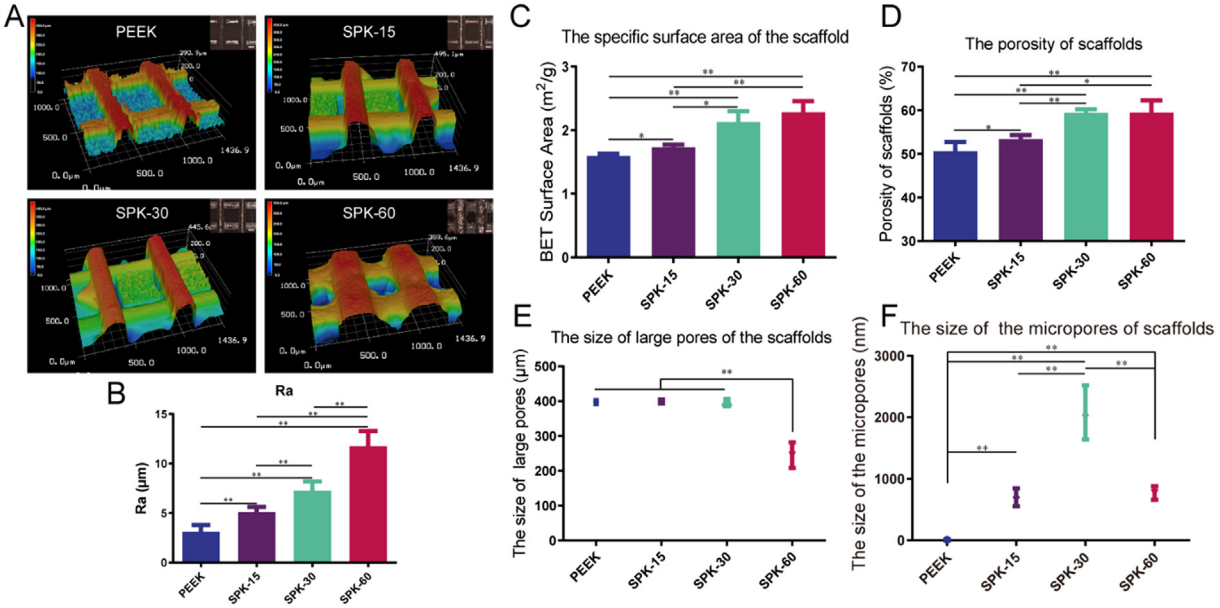

Figure 3. Structural analysis of scaffolds. A. Laser confocal microscopy of the surface morphology of different scaffolds. B. Surface roughness of different scaffolds. C. The specific surface area of different scaffolds. D. The porosity of different scaffolds. E. The large pore size (μm) of different scaffold. F. The micropore size (nm) of different scaffolds. Data are expressed as the mean ± SD (n = 5, one-way ANOVA, *P < 0.05, **P < 0.01).

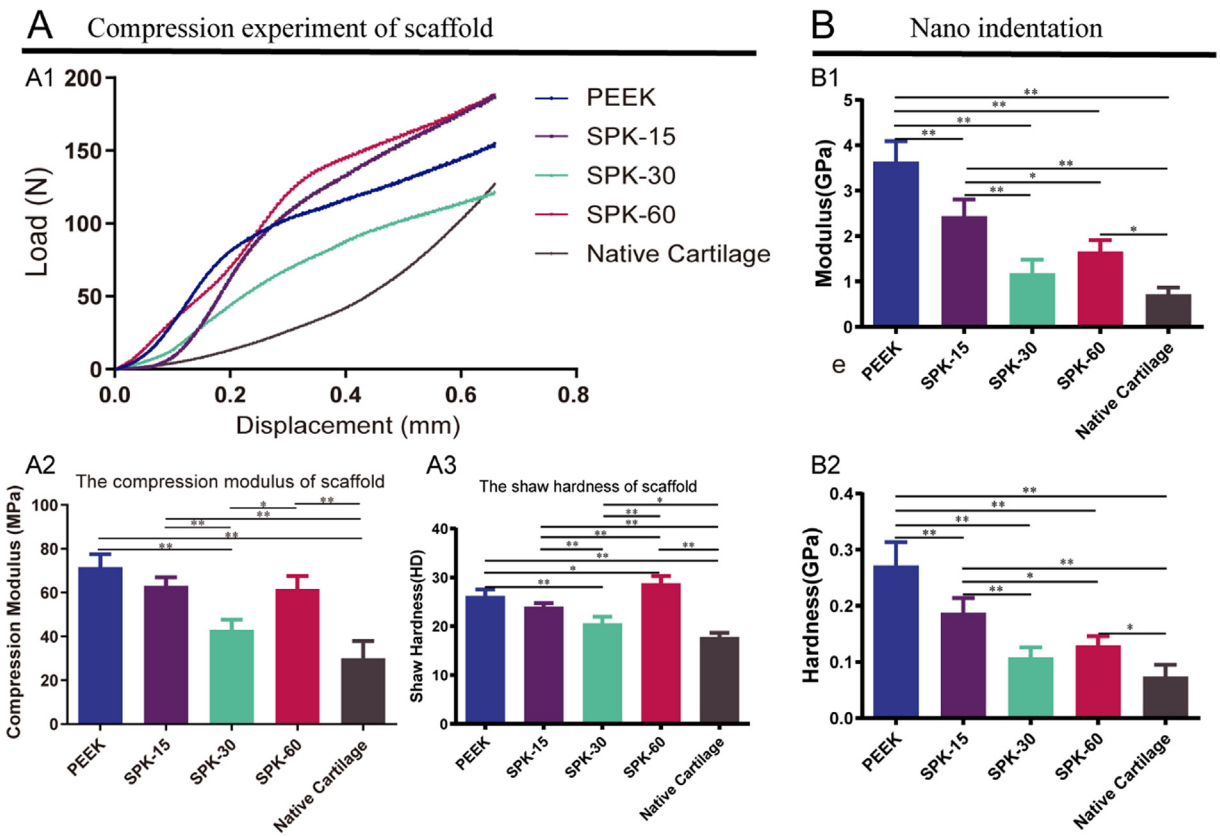

Figure 4. Biomechanical analysis of scaffolds. A. The bulk mechanical properties of different scaffolds, A1. The compression stress–strain diagrams of different scaffolds, A2. The compression modulus of different scaffolds, A3. The hardness of different scaffolds. B. The surface mechanical properties of different scaffolds via nanoindentation, B1. Compression modulus of different scaffolds, B2. Hardness of different scaffolds. Data are expressed as the mean ± SD (n = 5, one-way ANOVA, *P < 0.05, **P < 0.01, The native cartilage harvested from the donor served as a native control).

and was closer to that of native cartilage than the other three scaffolds (P < 0.05). The hardness of the samples showed similar results; the hardness of SPK-30 had the lowest compressive modulus of the four groups (P < 0.05).

Nanoindenter experiments were used to observe the surface biomechanical properties of these scaffolds (Fig. 4B). The PEEK scaffold had the maximum compressive modulus and hardness. The SPK-30 scaffold had the lowest compressive modulus and hardness, which were similar to those of the native cartilage. Meanwhile, the modulus and hardness of SPK-15 and SPK-60 were intermediate between those of the PEEK scaffolds and SPK-30 scaffolds, which showed a declining trend with the degree of sulfonation of PEEK, while the roughness and hardness increased dramatically as the degree of sulfonation of PEEK increased.

3.3. BSA adsorption capacity of scaffolds

The protein adsorption capacity of scaffolds may contribute to cell attachment, and was characterized in terms of the BSA content immobilized on the surface of PEEK, SPK-15, SPK-30, and SPK-60 at different times (Fig. 5A). Fig. 5B shows the BSA-FITC (green fluorescence) in different samples treated with BSA-FITC for 5 min. The protein adsorption capacities of SPK-30 and SPK-60 were superior to those of PEEK and SPK-15. From these results, we can conclude that the surface micro/nanostructure of sulfonated PEEK improved the protein adsorption ability.

3.4. Cytocompatibility of scaffolds in vitro

In this study, we evaluated the cytocompatibility of PEEK, SPK-15, SPK-30, and SPK-60 in this study. Chondrocyte viability on these different scaffolds was assayed via live/dead staining, where green indicates live cells and red indicates dead cells (Fig. 5C).

A large proportion of live chondrocytes adhered to the scaffolds, and we further tested cell viability, as shown in Fig. 5D. The results of the quantitative analysis showed that the cell viability of all four scaffolds reached more than 90%. We further tested the number of cells on scaffolds using ImageJ software, and the results showed that the number of cells on SPK-30 and SPK-60 was higher than that on PEEK and SPK-15 (P < 0.05) (Fig. 5E).

The cell adhesion capacity of a scaffold is a key factor that reflects its biocompatibility. In this study, we used CCK-8 to evaluate the attachment of chondrocytes on different scaffolds at 6, 12, 24, 48, and 72 h, and the proliferation of chondrocytes on scaffolds at 3, 7, and 14 days. The cell attachment of the different scaffolds is shown in Fig. 6A. From the increasing optical density (OD, the amount of cell adhesion) curve obtained from the different samples, we determined that the cell adhesion capacity of SPK-30 and SPK-60 is superior to that of PEEK and SPK-15. Fig. 6B shows that vinculin was expressed by chondrocytes on the scaffolds after 3 days of culture. This finding demonstrates that the chondrocytes spread very well on the surface, and the vinculin density on SPK-30 and SPK-60 was much higher than that on PEEK and SPK-15. These results suggest that the cells that grow on SPK-30 and SPK-60 have more anchoring points than those on PEEK and SPK-15 owing to the coarse nanotopography structure on the SPK-30 and SPK-60 surfaces. Fig. 6C shows the cell proliferation on the scaffolds after 3, 7, and 14 days. The SPK-30 and SPK-60 scaffolds significantly upregulated cell proliferation compared to the PEEK and SPK-15 scaffolds. Fig. 6D, E, and F show the quantitative analysis of collagen I and II, and glycosaminoglycan (GAG) secreted by chondrocytes on different scaffolds. The collagen I, II, and GAG increased over time for each of the four different scaffolds. Since

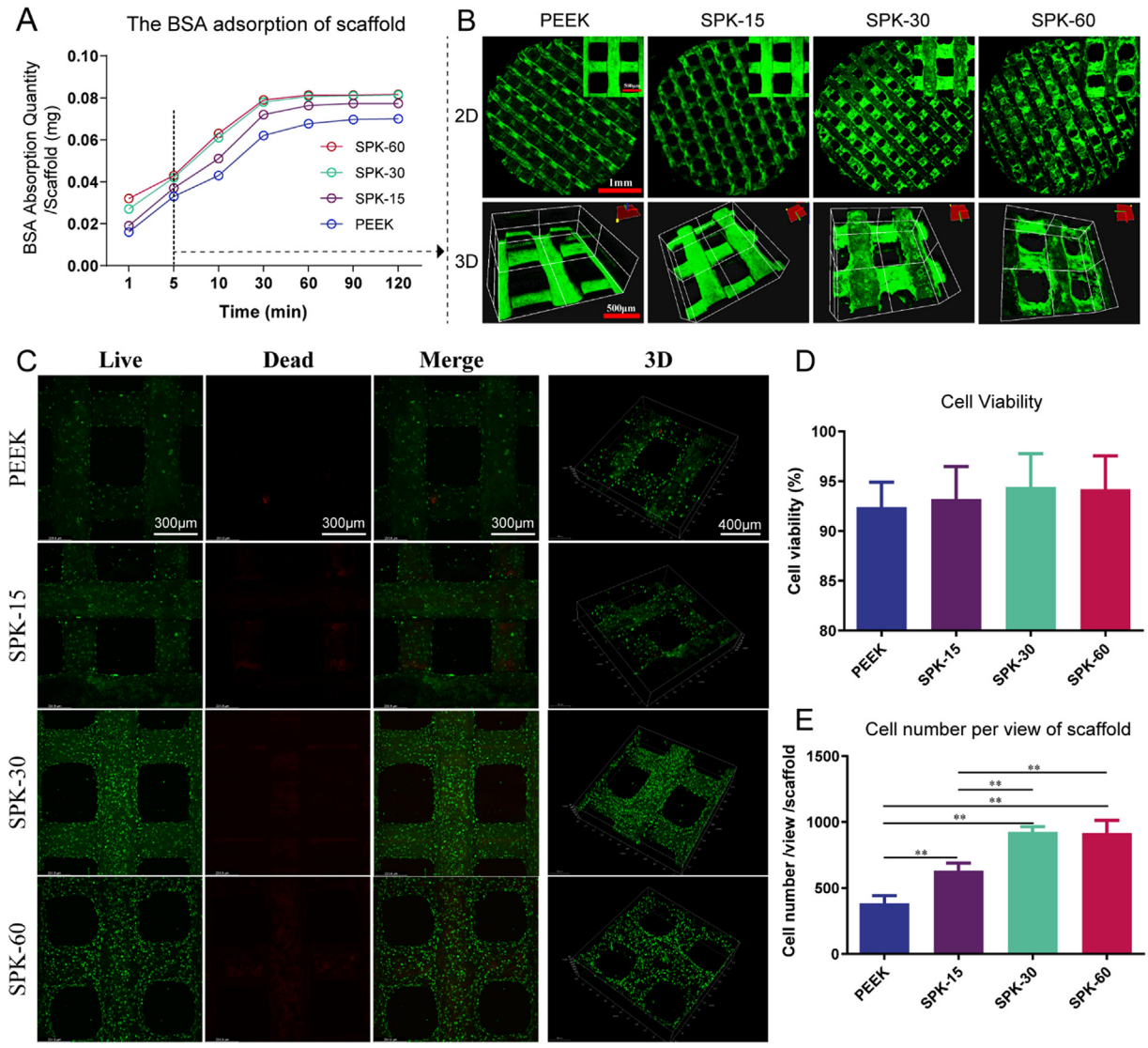

Figure 5. The BSA adsorption capacity and Live/Dead staining of samples. A. The protein adsorption curves of different samples. B. The fluorescent images of BSA-FITC on PEEK, SPK-15, SPK-30, and SPK-60. C. Live/dead staining of chondrocytes cultured on different scaffolds for 3 days. D. Viability analysis for the chondrocytes on different samples. E. The number of chondrocytes on different samples. Data are expressed as the mean ± SD (n = 5, one-way ANOVA, *P < 0.05, **P < 0.01).

ECM is often released in the media when chondrocytes are in culture, COL I, II, and GAG content were measured as that present in the media and scaffolds. The COL I content (scaffold + media) on PEEK, SPK-15, SPK-30, and SPK-60 increased by 70, 68, 52, and 57% at 7 days, and by 198, 175, 143, and 151%, respectively, at 14 days compared with that at 3 days. COL I deposition on the SPK-30 and SPK-60 was higher than that on the PEEK and SPK-15. COL II deposition on the SPK-30 and SPK-60 was higher than that on the PEEK and SPK-15 at 3, 7, and 14 days of culture, and COL II content (scaffold + media) on PEEK, SPK-15, SPK-30, and SPK-60 scaffolds increased by 58, 61, 69, and 68% at 7 days, and by 176, 184, 200, and 192% at 14 days, respectively, compared with that at 3 days. Similar to COL II, the total GAG content on SPK-30 and SPK-60 was higher than that on PEEK and SPK-15 (Fig. 6F). The total GAG (scaffold + media) increased by 62, 65, 76, and 74% at 7 days, and by 210, 219, 247, and 240% at 14 days compared with that at 3 days for the PEEK, SPK-15, SPK-30, and SPK-60 scaffolds, respectively.

3.5. Macrophages polarization modulating effect of scaffolds

3.5.1. Immunofluorescence staining of macrophages treated with scaffolds

The iNOS and CD206 expression of macrophages (RAW264.7) cultured on PEEK, SPK-15, SPK-30, and SPK-60 scaffolds for 4 days was monitored by immunofluorescence staining. The results are shown in Fig. 7A, which indicated that the inducible nitric oxide (iNOS) (M1 marker) was highly expressed in the PEEK group and low in the SPK-15, SPK-30, and SPK-60 groups; CD206 (M2 marker) was low in the PEEK group and highly expressed in the SPK-15, SPK-30, and SPK-60 groups. These results suggest that sulfonated PEEK (SPK-15, SPK-30, and SPK-60) can inhibit the expression of iNOS and enhance the expression of CD206 in macrophages (RAW264.7) compared to PEEK.

3.5.2. Gene expression of macrophages treated with scaffolds

To further evaluate the capacity of these scaffolds to exert macrophage polarization effects, we used reverse transcriptase polymerase chain reaction (RT-PCR) to further evaluate the expression of representative genes (CCR7, IL-1, iNOS, and CD206) of macrophages cultured on PEEK, SPK-15, SPK-30, and SPK-60. As shown in Fig. 7B (B1–4), the M2 macrophage marker CD206 was upregulated on SPK-15, SPK-30, and SPK-60 at 1 and 4 days compared to PEEK ($P < 0.05$), and the levels of inflammatory genes CCR7, IL-1, and iNOS were reduced in the SPK-15, SPK-30, and SPK-60 groups compared with the PEEK group, while there was no significant difference among the SPK-15, SPK-30, and SPK-

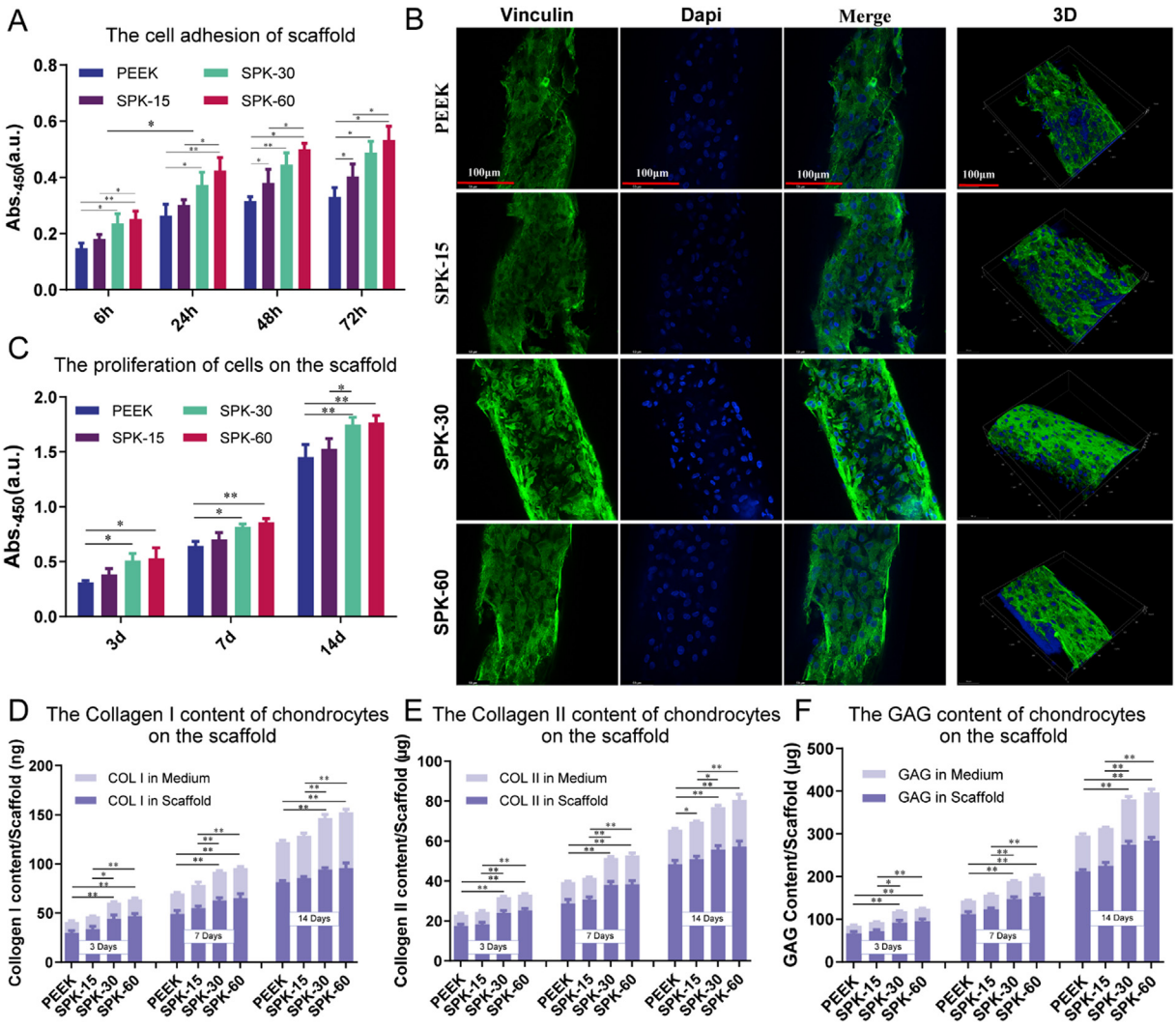

Figure 6. Adhesion, proliferation, and ECM secretion of chondrocytes on different samples. A. The adhesion analysis of chondrocytes on different scaffolds at 6, 24, 48, and 72 h (n = 5, two-way ANOVA, *P < 0.05, **P < 0.01). B. The vinculin immunofluorescence of chondrocytes on different scaffolds for 3 days. C. The proliferation analysis of chondrocytes on different scaffolds. D. The total collagen I secreted by chondrocytes on different scaffolds. E. The total collagen II secreted by chondrocytes on different scaffolds. F. The total glycosaminoglycan (GAG) secreted by chondrocytes on different scaffolds. Data are expressed as the mean ± SD (n = 5, one-way ANOVA, *P < 0.05, **P < 0.01).

60 groups. These results indicate that sulfonated PEEK (SPK-15, SPK-30, and SPK-60) may have anti-inflammatory effects.

3.5.3. *Cytokine secretion of macrophages seeded on these scaffolds*

These cytokines (including TNF-α, IL-1β, IL-4, and IL-10) secreted by macrophages (RAW264.7) cultured on PEEK, SPK-15, SPK-30, and SPK-60 for 1 and 4 days were measured using ELISA. The results are shown in Fig. 7C(C1–4), which indicated that compared to the macrophages on PEEK at 1 and 4 days, the macrophages on SPK-15, SPK-30, and SPK-60 secreted higher amounts of anti-inflammatory cytokines (interleukin (IL)-4 and IL-10) (P < 0.05), while they produced lower levels of inflammatory cytokines (TNF-α and IL-1β), which are mainly produced by M1 macrophages. Moreover, TNF-α, IL-1β, IL-4, and IL-10 concentrations of RAW264.7 cultured on SPK-15, SPK-30, and SPK-60 showed no significant difference. These findings are consistent with the RT-PCR results.

3.6. *Cartilage degeneration induced by macrophages treated with PEEK and SPK*

To further evaluate the capacity of the scaffolds for cartilage protection, we utilized the trans-well system to co-culture chondrocyte pellets and macrophages (RAW264.7) treated with PEEK and SPK. After co-culturing for 1 week, the pellets were harvested and evaluated. Fig. 7E shows the gross observation of these pellets in the PEEK, SPK, and control groups. The DNA content of the pellets was not significantly different between the PEEK, SPK, and control groups (Fig. 7F). The GAG/DNA of the pellets in the SPK and control groups was significantly higher than that in the PEEK group, while there was no significant difference between the SPK and control groups (Fig. 7G). We also observed the aggrecan, MMP 13 and collagen II in these pellets through immunofluorescence staining (Fig. 7H). Aggrecan and Collagen II were highly expressed in the SPK and control groups, and low in the PEEK group, whereas MMP 13 was expressed at low levels in the SPK and control groups, and highly expressed in the PEEK group. Generally, these results indicate that SPK may be able to prevent cartilage degeneration induced by macrophages by regulating macrophage polarization.

3.7. *Results of in vivo rabbit chondral defect model*

3.7.1. *Macroscopic evaluation*

In the present study, we evaluated the efficacy of 3D printed porous PEEK and SPK scaffolds for the treatment of chondral defects at 3, 6, and

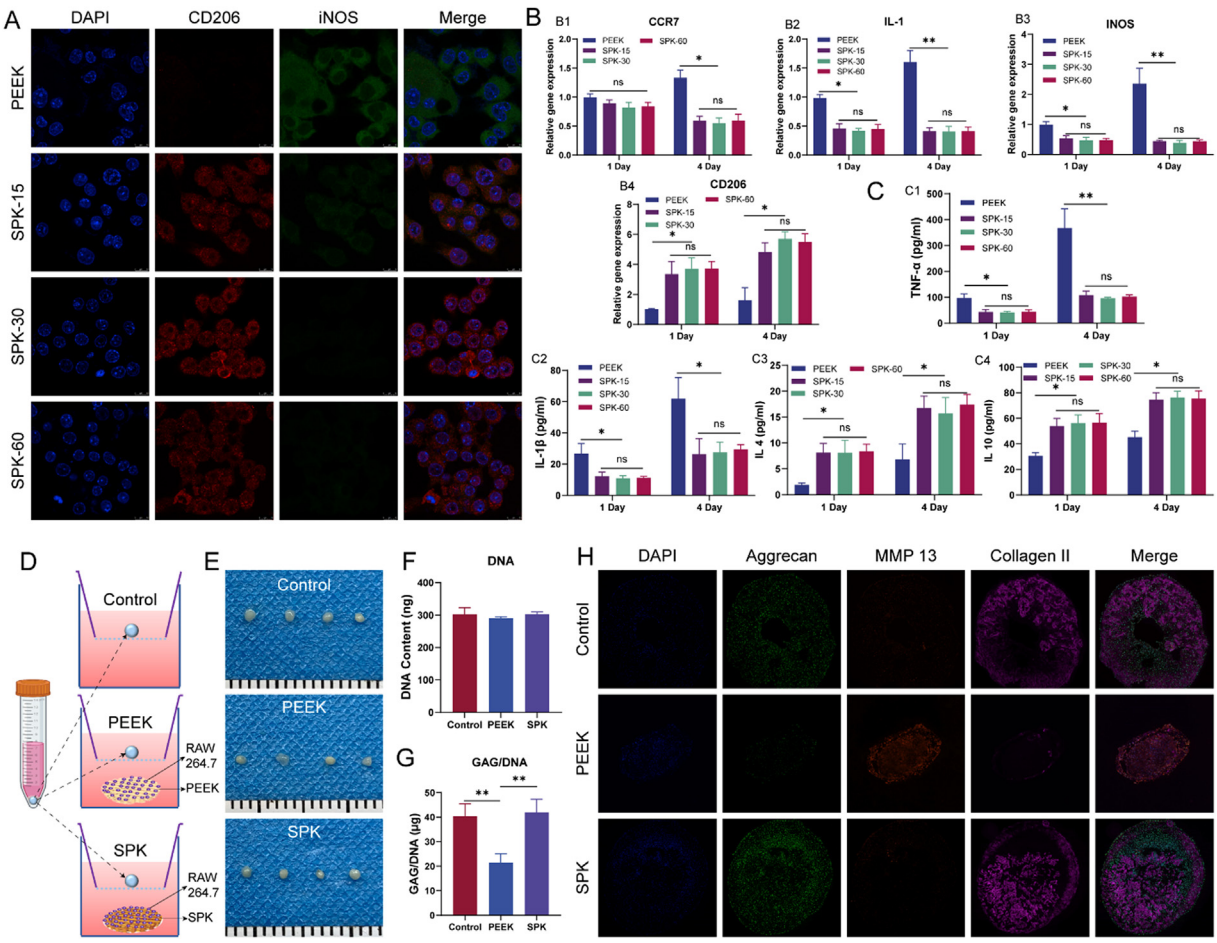

Figure 7. Macrophage polarization modulating effect and cartilage protection analysis of scaffolds. A. Immunofluorescence staining of macrophages (RAW264.7) cultured with PEEK, SPK-15, SPK-30 and SPK-60 for 4 days. B. The inflammation related genes expression of macrophages (RAW264.7) cultured on PEEK, SPK-15, SPK-30 and SPK-60 for 1 and 4 days, showing the results for CCR7 (B1), IL-1 (B2), INOS (B3), and CD206 (B4). C. The inflammation related cytokines secretion of macrophages (RAW264.7) cultured on PEEK, SPK-15, SPK-30 and SPK-60 for 1 and 4 days, showing the results for TNF-α(C1), IL-1β (C2), IL-4 (C3), and IL-10 (C4). Data are expressed as the mean ± SD (n = 5, one-way ANOVA, *P < 0.05, **P < 0.01). D-H. Cartilage degeneration induced by macrophages treated with PEEK and SPK for one week. D showed the general scheme, E showed the macroscopic observation of these chondrocytes pellets, F and G showed the DNA content and GAG/DNA of these chondrocytes pellets (n = 3, t test, **P < 0.01), H showed the immunofluorescence staining (Aggrecan, MMP13 and Collagen II) of these chondrocytes pellets.

12 weeks. Macroscopically, the defects were repaired with scaffolds and new tissue in both PEEK and SPK scaffolds. Meanwhile, the smoothness of the articular surface and the integration of scaffolds with host tissues varied in the PEEK and SPK groups (Fig. 8 A). We utilized a modified semiquantitative scoring of macroscopic cartilage repair to evaluate the repair effect of PEEK and SPK for chondral defects, and we used the untreated group as a control group. In terms of macroscopic scoring, we evaluated the repair effect of PEEK and SPK scaffolds; all macroscopic scoring parameters are shown in Fig. 8 B1–B6. These macroscopic scoring results demonstrate that the cartilage repair effect of SPK was much better than that of PEEK and the control group.

3.7.2. Histological analyses

3.7.2.1. Hard tissue slicing analyses for tissue integration of the scaffolds. Tissue integration of the scaffolds was evaluated using hard tissue slicing stained with toluidine blue (TB) (Fig. 8C). The percentage of tissue-scaffold contact (TSC), new tissue growth into the scaffold (NTIS), and bone-scaffold contact (BSC) were calculated according to histological images. The results show that the TSC (Fig. 8D) and NTIS (Fig. 8E) of the SPK group were much higher than those of the PEEK group at 3 weeks. The BSC of the SPK group was much higher than that of the PEEK group at 3, 6, and 12 weeks (Fig. 8F).

The SEM images and element evaluations are shown in Fig. 9. The gap between the scaffold and host tissue could still be clearly visible in the PEEK group 3 weeks post-implantation, but could hardly be observed in the SPK group. The EDS results confirmed that new fibrous tissue formed in the PEEK scaffold, and some new bone grew into the SPK scaffold.

3.7.2.2. Histological analyses of peri-scaffold cartilage. We evaluated peri-scaffold adjacent cartilage degeneration using HE, SO/FG, and Masson staining (Fig. 10A). According to the present results, the cartilage adjacent to the defect with or without scaffold treatment showed signs of degeneration, such as cartilage fibrillation or fissuring, chondrocyte necrosis, and clusters. To conduct semi-quantitative analysis of cartilage degeneration, we used the OARSI score to observe the effects of defects with or without scaffolds on the adjacent cartilage. The results showed that the OARSI scores of cartilage located at the peri-scaffold in the SPK group were better than those in the PEEK and control groups at 3, 6, and 12 weeks (P < 0.05) (Fig. 10B and C).

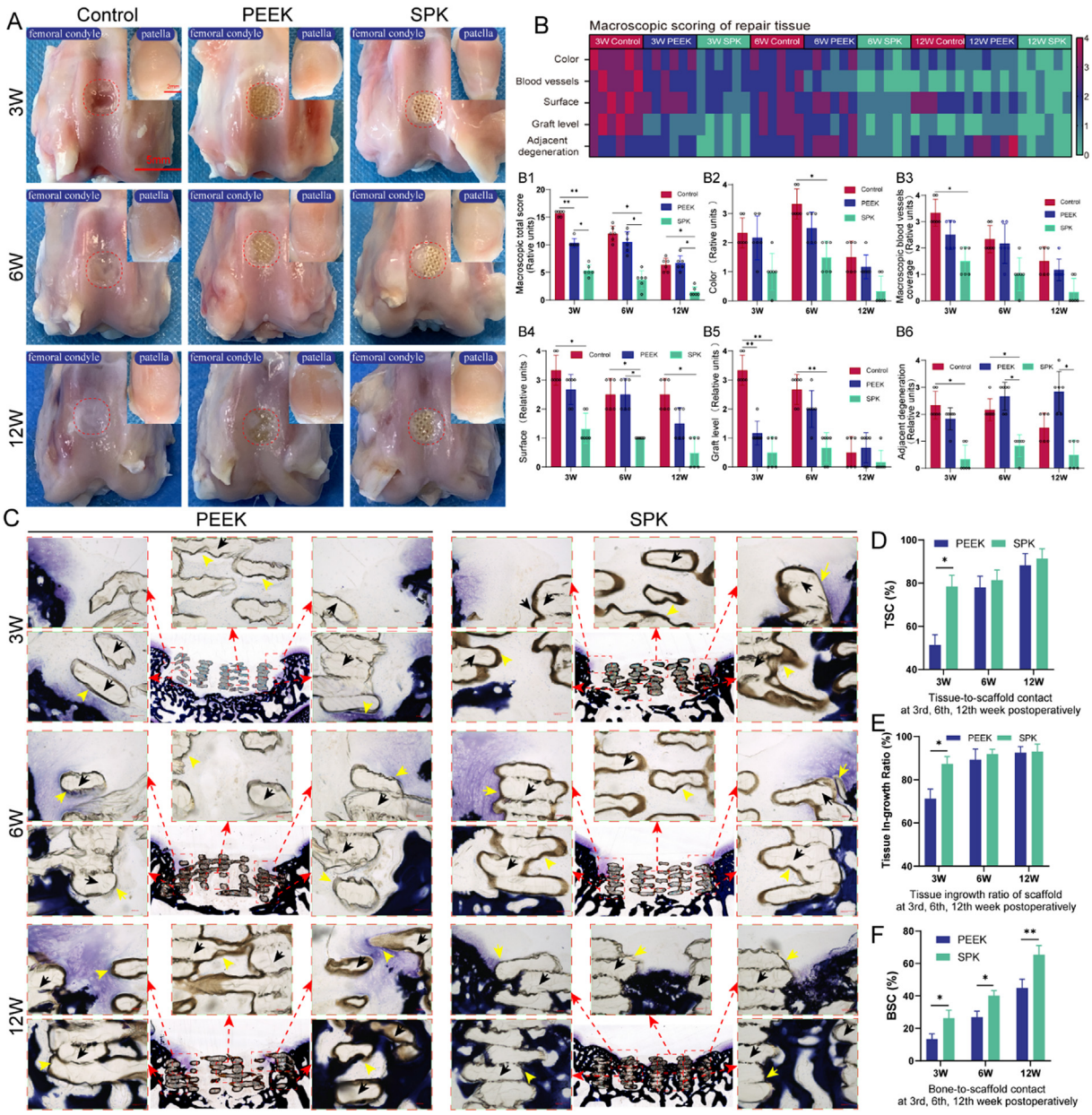

Figure 8. Macroscopic and histological analyses of cartilage repair with PEEK and SPK scaffolds treatment in cartilage defects at 3, 6, and 12 weeks postoperatively. A. Macroscopic views. B. Heat map of variables. B1–B6. The variables analysis of the macroscopic scoring. B1. Macroscopic total score. B2. Macroscopic color score. B3. Macroscopic blood vessel coverage. B4. Macroscopic surface score. B5. Graft level score. B6. Adjacent cartilage degeneration score. Data are expressed as the mean ± SD, n = 6, one-way ANOVA, *P < 0.05, **P < 0.01. C. Toluidine blue staining of samples. Black arrow indicates PEEK or SPK scaffolds, yellow arrow indicates the interface of new tissue and scaffolds. D. The percentage of tissue-scaffold contact (TSC) was computed by the length of the new tissue contact with the scaffold. E. The NTIS was calculated by the proportion of new tissue growth into the scaffold. F. The bone-scaffold contact (BSC) was computed with the length of the bone in contact with the scaffold. All data were determined according to the analysis of histological images by three investigators and expressed as the mean ± SD (n = 3, t test, *P < 0.05, **P < 0.01).

3.7.3. *Micro-CT analysis*

We utilized micro-CT to characterize the defect with new tissue ingrowth, and new bone in the repair area was constructed (Fig. 11A). The results showed that the new bone formation in the SPK group was much greater than that in the PEEK and control groups. BMD, BV/TV, and Tb.N were used to determine the repair of subchondral bone introduced by PEEK and SPK. We found that the SPK group had the highest bone mineral density (BMD) in the repair area compared to the PEEK and control groups (Fig. 11B). Similarly, both the BV/TV (Fig. 11C) and Tb.N (Fig. 11D) of the SPK group were significantly higher than those of the other two groups.

3.7.4. *Biomechanical analysis*

In this study, a pull-out test was conducted to evaluate the tissue integration capacity of PEEK and SPK at 3, 6, and 12 weeks after surgery. The interface bonding strength between the scaffold and tissue showed

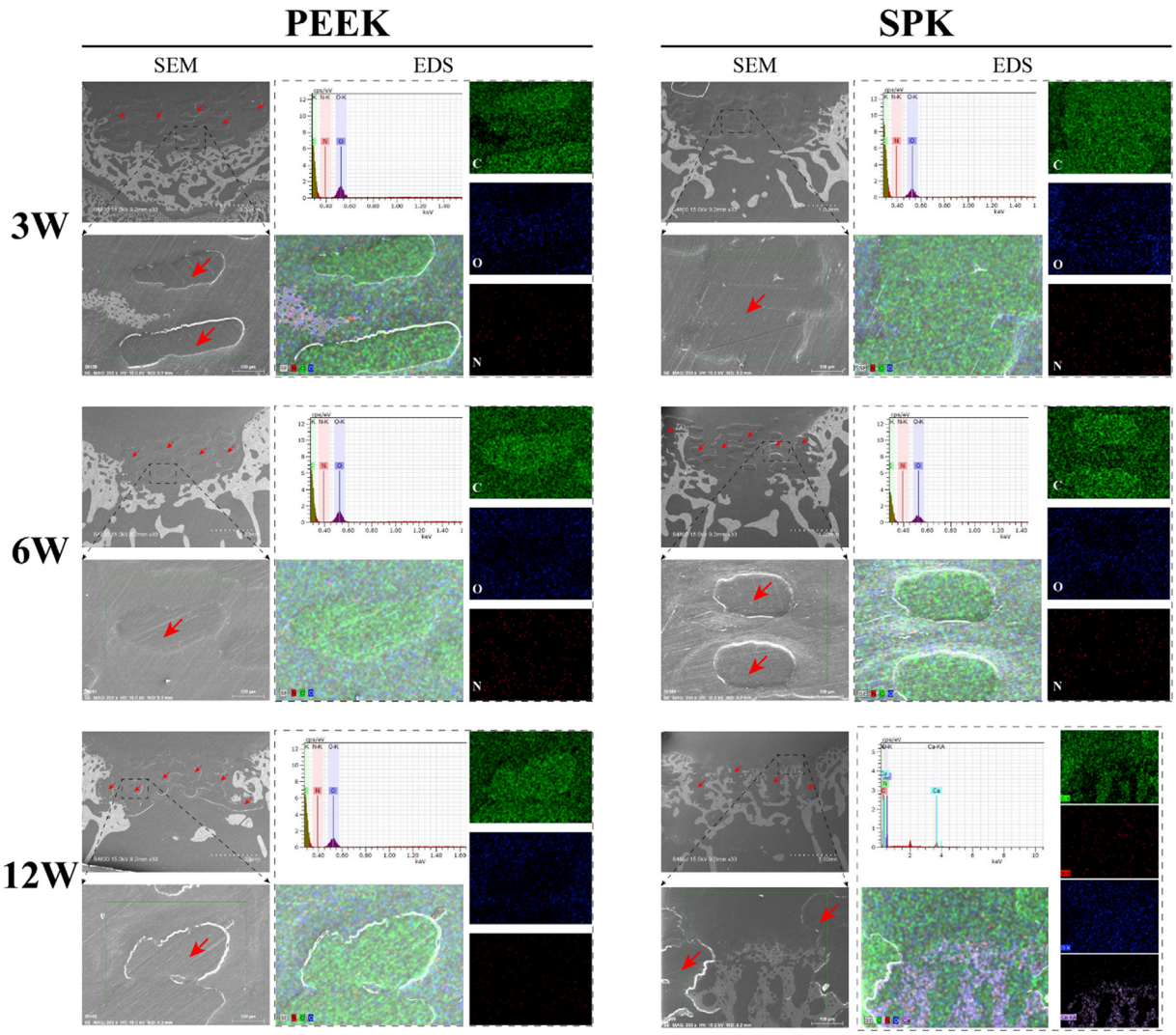

Figure 9. SEM and EDS analysis for the samples in the PEEK and SPK groups at three, six, and 12 weeks postoperatively (red arrow indicates the PEEK or SPK scaffolds).

an increasing trend with time for each group, and the interface bonding strength was significantly higher in the SPK group than in the PEEK group at 3, 6, and 12 weeks after surgery (Fig. 11E).

We also used compression tests to investigate the compressive modulus of the repair tissue with a scaffold. The compression modulus of repair tissue with scaffold (PEEK or SPK) was much higher than that of the repair tissue without scaffold (control group). The compression modulus of repair tissue with SPK scaffold in the SPK group, close to the modulus of native tissue, was lower than that of the PEEK scaffold in the PEEK group at each time point (Fig. 11F).

3.7.5. The chondroprotective effect of scaffolds for patella

We evaluated the protective effect of PEEK and SPK scaffolds on the rabbit knee joint through gross observation and histological analysis of the contralateral patellar cartilage. Macroscopic observation showed no obvious morphological changes to the cartilage in the SPK group, while the patellar cartilage surface was incomplete and rougher in the PEEK and control groups. We utilized HE, TB, and SO/FG staining to observe the progression of cartilage degeneration in the contralateral patella (Fig. 12A). Based on the results, chondral degeneration progressively exacerbated over time in all the PEEK, SPK, and control groups, and the chondroprotective effect of the SPK scaffold was much better than that of the PEEK scaffold. Semi-quantitative analysis for histological staining showed that the Mankin score of the contralateral patellar cartilage in the SPK group was better than that in the PEEK and control groups at 3, 6, and 12 weeks (Fig. 12B, C, D).

Next, we measured the changes in the inflammatory cytokines (IL-1β and TNF-α) in the rabbit knee joint fluid using an ELISA kit. The results showed that the IL-1β (Fig. 12E) and TNF-α (Fig. 12F) contents in the knee joint fluid were significantly lower in the SPK group than in the PEEK and control groups. Overall, the SPK scaffold showed better chondroprotective effects on the contralateral patellar cartilage and produced fewer inflammatory cytokines in the knee joint fluid than the PEEK scaffold.

4. Discussion

For current cartilage tissue engineering strategies, the elderly are not appropriate because of their weak regenerative potency [34]. At present, there is no specific treatment for elderly patients with FCDs, leading to the development of OA and necessitating joint replacement [35]. In this study, we first propose a new cartilage repair strategy based on a

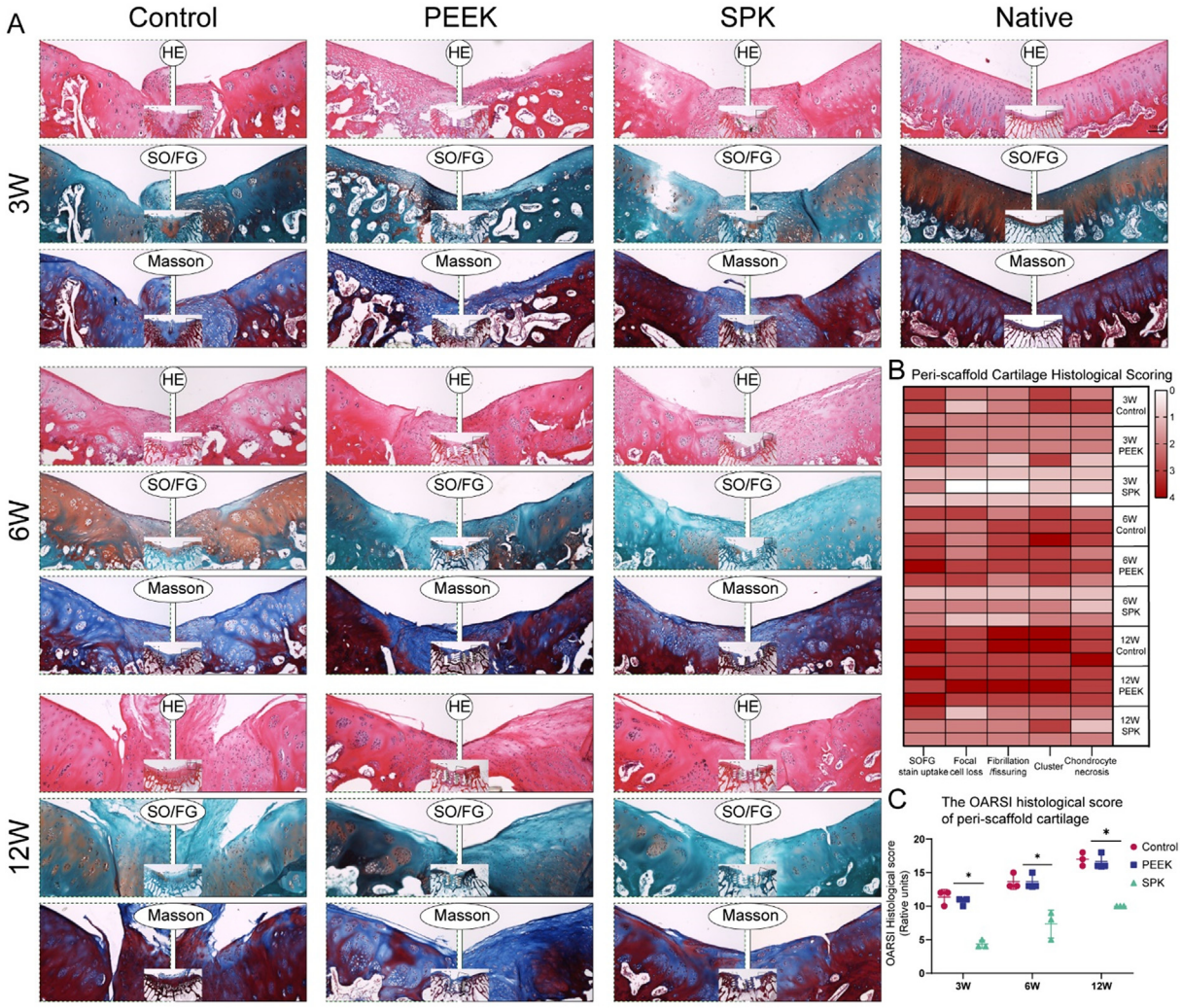

Figure 10. Histological analyses of peri-scaffold cartilage. A. HE, SO-FG, and Masson staining of peri-scaffold cartilage. B. Heat map of variables of the histological OARSI scoring. C. Histological OARSI score. Data are expressed as the mean ± SD (n = 3, one-way ANOVA, *P < 0.05).

nondegradable porous sulfonated PEEK scaffold with multiple functions, which can provide appropriate mechanical support as a chondral prosthesis, can induce cartilage repair as a cartilage tissue engineering scaffold, has superior multifunctionality toward immunoregulation for macrophage polarization and cartilage protection, and can coexist with new tissue ingrowth.

In this study, we successfully fabricated 3D porous PEEK scaffolds via fused-filament fabrication. To the best of our knowledge, the surface micro/nanostructure of solid orthopedic implants can favor cell attachment and proliferation, even influencing later stages of tissue regeneration [36]. As PEEK is chemically and biologically inert, sulfonated treatment to fabricate a porous micro/nanostructure on the surface has been studied for decades [37]; however, the sulfonation of 3D printed PEEK scaffolds has not been studied before. In this study, we treated the 3D printed porous PEEK scaffolds with concentrated sulfuric acid for 15 s (SPK-15), 30 s (SPK-30), and 60 s (SPK-60). As the sulfonated treatment time increased, the surface morphology, elemental composition, and chemical groups of the samples were detected by SEM, EDS, XPS, and FTIR. The SEM results showed that the SPK-30 scaffold had a superior micro/nano pore structure and a homogeneous, hierarchical, and interconnective surface topography compared with the SPK-15 and SPK-60 scaffolds. The EDS and XPS results confirmed that the sulfur content increased over the treatment time, whereas the sulfur content of all the sulfonated PEEK was below 1%, which is considered safe for cell adhesion and proliferation. FTIR spectra confirmed that SO_3H functional groups were immobilized on the SPK surface by sulfonation.

As an effective surface modification method, sulfonation can not only fabricate micro- and nanoscale pores on the surface to enhance the surface area and porosity of PEEK, but can also change the surface mechanical properties, especially for 3D printed porous PEEK scaffolds. The results of the compression and nanoindentation experiments show that the trend of the bulk compressive modulus of samples with sulfonation time is consistent with that of the surface compressive modulus of the samples. With the extension of sulfonation time, the compressive modulus of the samples first decreased and then increased, which corresponded to the surface topography of the scaffolds. The biomechanical tests showed that the modulus and hardness of SPK-30 were lower than those of PEEK, SPK-15, and SPK-60, which is closer to that of native cartilage. It is well known that surface microtopography of solid orthopedic implants enhances cell attachment, proliferation, and osseointegration [38]. In this study, we evaluated the biofunctionalities of adhesion, proliferation, and cell phenotypic maintenance of PEEK and

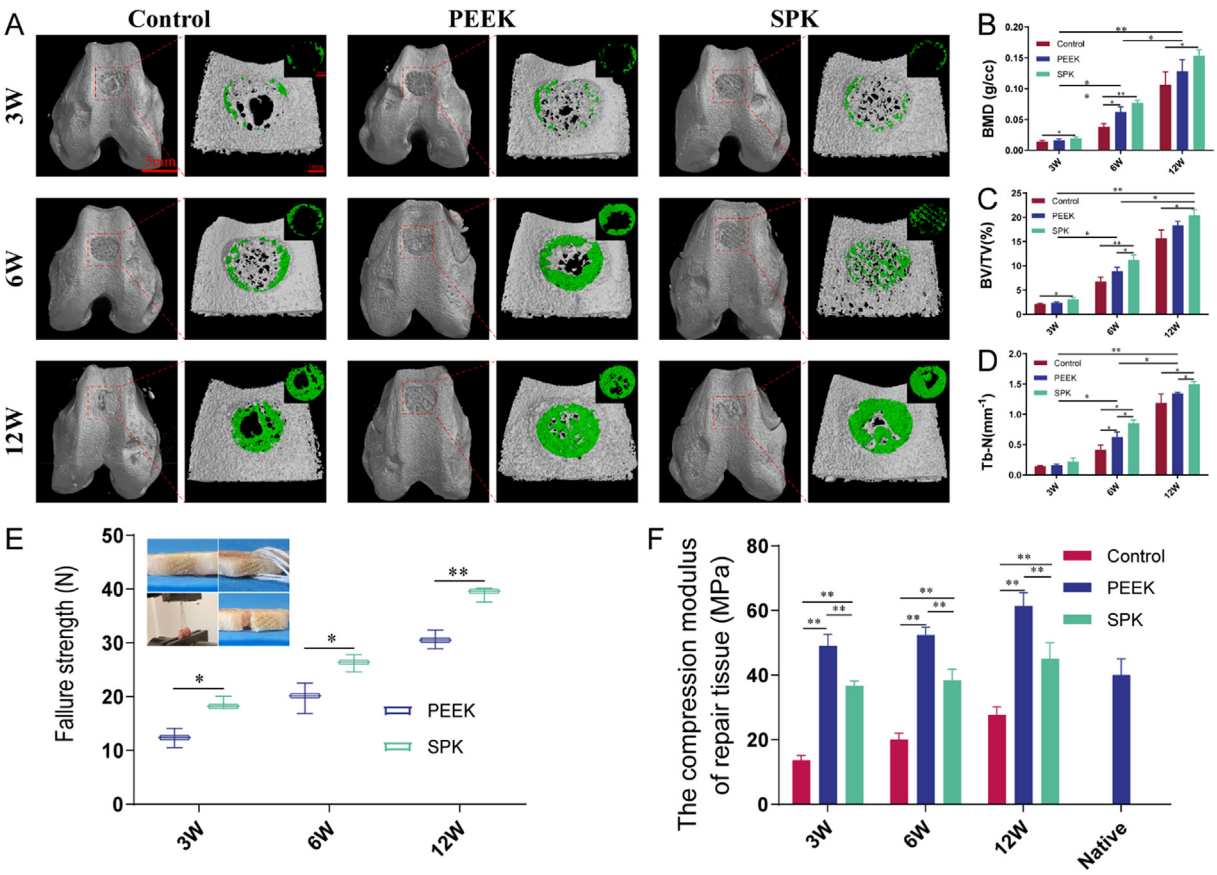

Figure 11. Micro-CT and biomechanics analysis. A. 3D reconstructed images from micro-CT for PEEK and SPK implantation in vivo (green part represents newly formed bone). B-D. Quantitative analysis of BMD (B), BV/TV (C), and Tb.N (D). Data are expressed as the mean ± SD (n = 3, two-way ANOVA, *P < 0.05, **P < 0.01). E–F. Pull-out loads (E) of the samples, and compressive modulus (F) of repair tissue with scaffold. Data are expressed as the mean ± SD (n = 3, one-way ANOVA, *P < 0.05, **P < 0.01).

sulfonated PEEK using chondrocytes. According to our results, sulfonation can significantly enhance BSA adhesion, chondrocyte attachment, proliferation, and cartilage extracellular matrix secretion. The SPK-30 scaffold was the best among the three sulfonated PEEK scaffolds (SPK-15, SPK-30, and SPK-60), which was consistent with the results of the surface topography. Although the reason for the cell response to the micro/nanoscale topography of biomaterials is not very clear, some previous studies suggest that the micro/nanoscale topography of biomaterials could influence cell behaviors by changing the integrin-binding proteins and related integrin signaling. Recent literature suggests that macrophages can contribute to the modulation of joint inflammation, thereby modulating OA severity [39]. New approaches that can manipulate macrophage polarization may provide a novel approach for preventing OA or promoting chondral repair. Older patients with focal cartilage lesions often have OA [40]. Recently, some studies have demonstrated that varying the surface topography of biomaterials can modulate their response to macrophages [41]. In this study, we investigated the macrophage polarization modulating capacity of sulfonated PEEK (SPK-15, SPK-30, and SPK-60) and their anti-inflammatory effects. According to the present results, compared to PEEK, all three sulfonated PEEK scaffolds can favor macrophage polarization to M2 and enhance anti-inflammatory cytokine secretion. Some previous studies have reported that porous micro/nanostructures can favor macrophage adhesion and spread, modulating the local microenvironment and macrophage polarization [42,43] However, in this study, we found that there were no significant differences during SPK-15, SPK-30, and SPK-60 for their macrophage polarization modulating ability and anti-inflammatory effects in spite of their different surface micro/nanostructures, which are shown in Fig. 1. Therefore, we suggest that the micro/nanostructure and sulfonic acid groups produced by the sulfonated treatment may contribute to macrophage polarization regulation. Furthermore, we observed the chondrocyte protective effects of PEEK and SPK through a co-culture system. The chondrocyte pellets in the SPK group expressed high levels of aggrecan and collagen II and lowly expressed MMP 13, compared to those in the PEEK group. Thus, the present study confirmed that sulfonated PEEK could prevent macrophage-induced cartilage degeneration *in vitro* by polarizing macrophages to the M2 phenotype, which inhibited inflammatory cytokine secretion.

Next, we systematically evaluated the feasibility and safety of PEEK and sulfonated PEEK chondral scaffolds as a treatment for local chondral defects in a rabbit model. Macroscopically, the smoothness and integration of scaffolds with host tissues were better in the SPK group than in the PEEK and control groups. Histologically, we evaluated tissue ingrowth and integration of scaffolds via TSC, NTIS, and BSC based on hard tissue sections. These results demonstrated that the SPK scaffold can better promote tissue ingrowth and integration than the PEEK scaffold, which was also confirmed by a pull-out test. The SPK scaffold was found to be more effective in preventing peri-scaffold cartilage degeneration, patellar cartilage degeneration, and inflammatory cytokine expression compared with the PEEK scaffold. Furthermore, the micro-CT results confirmed that the SPK scaffold can better favor subchondral bone repair than the PEEK scaffold, and the compressive test results showed that the compressive modulus of the repaired tissue with the SPK scaffold was superior to that of the PEEK group. Overall, as a better chondral

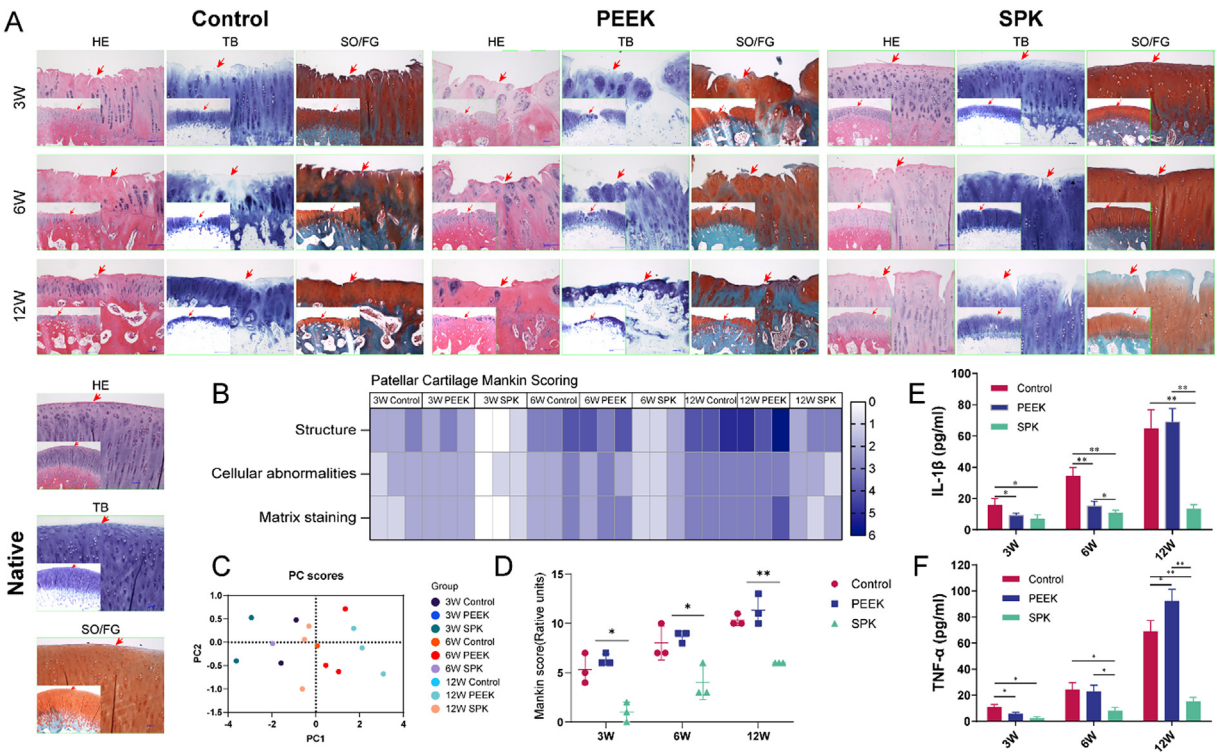

Figure 12. The protective analysis of PEEK and SPK for the knees of rabbits with full-thickness chondral defects. A. Histological staining of contralateral patellar cartilage to the defects. B. Heat map of variables of the Mankin histological scoring. C. PCA of total Mankin score. D. The total Mankin histological score. E and F. Expression of the inflammatory cytokines IL-1β (E) and TNF-α (F) in synovial fluid of the knee joint. Data are expressed as the mean ± SD (n = 3, one-way ANOVA, *P < 0.05, **P < 0.01).

functional replacement compared to the PEEK scaffold, the SPK scaffold can promote tissue ingrowth and integration, prevent peri-scaffold and patellar cartilage degeneration, and inhibit inflammatory cytokine expression, which may be related to its physicochemical, biomechanical, biofunctional, and anti-inflammatory properties.

Despite our efforts, the present study has some disadvantages. First, a limition of this study is the lack a mechanical sheer/sliding test of the constructs against cartilage plugs, even if the in-vitro mechanical test hardly simulates the real condition in vivo, it still is meaningful, and will be performed in our next study. Second, the rabbit model is also a drawback of this study; the rabbit knee is bent, and thus very different from the human knee joint. In addition, rabbits have a greater tendency to undergo tissue regeneration. Furthermore, as a 3D printed scaffold with translational potential, some more issues need to be clarified, such as the residue of the scaffolds [44], long term stability and safety of the scaffolds in vivo [45,46].

To the best of our knowledge, this study is the first successful in vivo application of a non-degradable biomaterial-guided restoration of cartilage function in a cartilage defect animal model. This study shows that sulfonated PEEK significantly improves the functional restoration of cartilage defects. Compared to PEEK, SPK scaffolds can mimic the biomechanical properties of native cartilage, promote cell attachment and proliferation, modulate macrophage polarization and exert anti-inflammatory effects, prevent macrophage-induced chondrocyte degeneration *in vitro,* promote tissue ingrowth and integration, and prevent cartilage degeneration and inflammatory cytokine secretion in vivo. All these findings suggest that the SPK scaffold may be a highly promising material for cartilage function replacement. Taken together, this study supports the concept of non-degradable material-guided cartilage function restoration as a promising therapeutic approach for elderly patients with FCDs, especially giant osteochondral defects. Moreover, PEEK has been approved by FDA for clinical application, and some PEEK based medical implants, such as PEEK Cerviacl Intervertebral Cage, PEEK OPTIMA, and so on. Therefore, from a clinical application perspective, such a PEEK based scaffold strategy would be promising for osteochondral defects in elderly patients with weak cartilage regeneration potential and may represent a major new avenue for elderly individuals with giant osteochondral defects.

5. Conclusions

In this study, the PEEK scaffold was fabricated via 3D printing for cartilage function restoration, and then surface-engineered with concentrated sulfuric acid for 15 s (SPK-15), 30 s (SPK-30), and 60 s (SPK-60). With sulfonated treatment, the scaffolds have good micro/nanostructure, appropriate biomechanical properties, superior biofunctionalities (chondrocyte adhesion, proliferation, and extracellular matrix secretion), favor macrophage polarization to M2 and anti-inflammatory cytokine expression, and prevent macrophage-induced cartilage degeneration *in vitro.*

An in vivo chondral repair study confirmed that the SPK scaffold favored excellent new tissue ingrowth and integration, prevented peri-scaffold cartilage degeneration, patellar cartilage degeneration, and inflammatory cytokine expression, and promoted cartilage function restoration.

In summary, the SPK scaffolds possessed good micro/nanostructure, appropriate biomechanical properties (close to native cartilage), cytocompatibility, new tissue ingrowth and integration capacity, cartilage protection, and anti-inflammatory effects, and therefore, have promising potential for chondral functional repair applications.

Funding sources

This study was supported by the National Key R&D Program of China (Grant No. 2016YFC1101802).

Declaration of interests

The authors declare that they have no known competing financial interests or personal relationships that could have appeared to influence the work reported in this paper.

Acknowledgment

Thanks Prof. Yu and Dr. Zhou from the Department of Anesthesiology, Renji Hospital, for providing technical support for CLSM.

References

[1] Becerra J, Andrades JA, Guerado E, Zamora-Navas P, Lopez-Puertas JM, Reddi AH. Articular cartilage: structure and regeneration. Tissue Eng B Rev 2010;16(6):617–27.
[2] Mankin HJ. The reaction of articular cartilage to injury and osteoarthritis (second of two parts). N Engl J Med 1974;291(25):1335–40.
[3] Kwon H, Brown WE, Lee CA, Wang D, Paschos N, Hu JC, et al. Surgical and tissue engineering strategies for articular cartilage and meniscus repair. Nat Rev Rheumatol 2019;15(9):550–70.
[4] Miller DJ, Smith MV, Matava MJ, Wright RW, Brophy RH. Microfracture and osteochondral autograft transplantation are cost-effective treatments for articular cartilage lesions of the distal femur. Am J Sports Med 2015;43(9):2175–81.
[5] Inderhaug E, Solheim E. Osteochondral autograft transplant (mosaicplasty) for knee articular cartilage defects. JBJS Essent Surg Tech 2019;9(4).
[6] Redondo ML, Beer AJ, Yanke AB. Cartilage restoration: microfracture and osteochondral autograft transplantation. J Knee Surg 2018;31(3):231–8.
[7] Gou GH, Tseng FJ, Wang SH, Chen PJ, Shyu JF, Weng CF, et al. Autologous chondrocyte implantation versus microfracture in the knee: a meta-analysis and systematic review. Arthroscopy 2020;36(1):289–303.
[8] Correa D, Lietman SA. Articular cartilage repair: current needs, methods and research directions. Semin Cell Dev Biol 2017;62:67–77.
[9] Campos Y, Almirall A, Fuentes G, Bloem HL, Kaijzel EL, Cruz LJ. Tissue engineering: an alternative to repair cartilage. Tissue Eng B Rev 2019;25(4):357–73.
[10] Huey DJ, Hu JC, Athanasiou KA. Unlike bone, cartilage regeneration remains elusive. Science 2012;338(6109):917–21.
[11] Liao J, Shi K, Ding Q, Qu Y, Luo F, Qian Z. Recent developments in scaffold-guided cartilage tissue regeneration. J Biomed Nanotechnol 2014;10(10):3085–104.
[12] Levingstone TJ, Thompson E, Matsiko A, Schepens A, Gleeson JP, O'Brien FJ. Multi-layered collagen-based scaffolds for osteochondral defect repair in rabbits. Acta Biomater 2016;32:149–60.
[13] Sun J, Tan H. Alginate-based biomaterials for regenerative medicine applications. Materials 2013;6(4):1285–309.
[14] Comblain F, Rocasalbas G, Gauthier S, Henrotin Y. Chitosan: a promising polymer for cartilage repair and viscosupplementation. Bio Med Mater Eng 2017;28(s1):S209–15.
[15] Pahoff S, Meinert C, Bas O, Nguyen L, Klein TJ, Hutmacher DW. Effect of gelatin source and photoinitiator type on chondrocyte redifferentiation in gelatin methacryloyl-based tissue-engineered cartilage constructs. J Mater Chem B 2019;7(10):1761–72.
[16] Ribeiro VP, Pina S, Oliveira JM, Reis RL. Silk fibroin-based hydrogels and scaffolds for osteochondral repair and regeneration. Adv Exp Med Biol 2018;1058:305–25.
[17] Narayanan G, Vernekar VN, Kuyinu EL, Laurencin CT. Poly (lactic acid)-based biomaterials for orthopaedic regenerative engineering. Adv Drug Deliv Rev 2016;107:247–76.
[18] Fan H, Hu Y, Zhang C, Li X, Lv R, Qin L, et al. Cartilage regeneration using mesenchymal stem cells and a PLGA-gelatin/chondroitin/hyaluronate hybrid scaffold. Biomaterials 2006;27(26):4573–80.
[19] Dahlin RL, Kinard LA, Lam J, Needham CJ, Lu S, Kasper FK, et al. Articular chondrocytes and mesenchymal stem cells seeded on biodegradable scaffolds for the repair of cartilage in a rat osteochondral defect model. Biomaterials 2014;35(26):7460–9.
[20] Jeuken RM, Roth AK, Peters R, Van Donkelaar CC, Thies JC, Van Rhijn LW, et al. Polymers in cartilage defect repair of the knee: current status and future prospects. Polymers 2016;8(6).
[21] Panayotov IV, Orti V, Cuisinier F, Yachouh J. Polyetheretherketone (PEEK) for medical applications. J Mater Sci Mater Med 2016;27(7):118.
[22] Wong KL, Wong CT, Liu WC, Pan HB, Fong MK, Lam WM, et al. Mechanical properties and in vitro response of strontium-containing hydroxyapatite/polyetheretherketone composites. Biomaterials 2009;30(23–24):3810–7.
[23] Makris EA, Responte DJ, Paschos NK, Hu JC, Athanasiou KA. Developing functional musculoskeletal tissues through hypoxia and lysyl oxidase-induced collagen cross-linking. Proc Natl Acad Sci U S A 2014;111(45):E4832–41.
[24] Custers RJ, Saris DB, Dhert WJ, Verbout AJ, van Rijen MH, Mastbergen SC, et al. Articular cartilage degeneration following the treatment of focal cartilage defects with ceramic metal implants and compared with microfracture. J Bone Joint Surg Am 2009;91(4):900–10.
[25] Waldorff EI, Roessler BJ, Zachos TA, Miller BS, McHugh J, Goldstein SA. Preclinical evaluation of a novel implant for treatment of a full-thickness distal femoral focal cartilage defect. J Arthroplasty 2013;28(8):1421–9.
[26] Custers RJ, Dhert WJ, Saris DB, Verbout AJ, van Rijen MH, Mastbergen SC, et al. Cartilage degeneration in the goat knee caused by treating localized cartilage defects with metal implants. Osteoarthritis Cartilage 2010;18(3):377–88.
[27] Kurtz SM, Devine JN. PEEK biomaterials in trauma, orthopedic, and spinal implants. Biomaterials 2007;28(32):4845–69.
[28] Yuan X, Ouyang L, Luo Y, Sun Z, Yang C, Wang J, et al. Multifunctional sulfonated polyetheretherketone coating with beta-defensin-14 for yielding durable and broad-spectrum antibacterial activity and osseointegration. Acta Biomater 2019;86:323–37.
[29] Ouyang L, Zhao Y, Jin G, Lu T, Li J, Qiao Y, et al. Influence of sulfur content on bone formation and antibacterial ability of sulfonated PEEK. Biomaterials 2016;83:115–26.
[30] Cavo M, Scaglione S. Scaffold microstructure effects on functional and mechanical performance: integration of theoretical and experimental approaches for bone tissue engineering applications. Mater Sci Eng C Mater Biol Appl 2016;68:872–9.
[31] Taniguchi N, Fujibayashi S, Takemoto M, Sasaki K, Otsuki B, Nakamura T, et al. Effect of pore size on bone ingrowth into porous titanium implants fabricated by additive manufacturing: an in vivo experiment. Mater Sci Eng C Mater Biol Appl 2016;59:690–701.
[32] Spece H, Yu T, Law AW, Marcolongo M, Kurtz SM. 3D printed porous PEEK created via fused filament fabrication for osteoconductive orthopaedic surfaces. J Mech Behav Biomed Mater 2020;109:103850.
[33] Goebel L, Orth P, Muller A, Zurakowski D, Bucker A, Cucchiarini M, et al. Experimental scoring systems for macroscopic articular cartilage repair correlate with the MOCART score assessed by a high-field MRI at 9.4 T–comparative evaluation of five macroscopic scoring systems in a large animal cartilage defect model. Osteoarthritis Cartilage 2012;20(9):1046–55.
[34] Zhao X, Bichara DA, Ballyns FP, Yoo JJ, Ong W, Randolph MA, et al. Properties of cartilage engineered from elderly human chondrocytes for articular surface repair. Tissue Eng 2012;18(13–14):1490–9.
[35] Fuggle NR, Cooper C, Oreffo ROC, Price AJ, Kaux JF, Maheu E, et al. Alternative and complementary therapies in osteoarthritis and cartilage repair. Aging Clin Exp Res 2020;32(4):547–60.
[36] Wu J, Li L, Fu C, Yang F, Jiao Z, Shi X, et al. Micro-porous polyetheretherketone implants decorated with BMP-2 via phosphorylated gelatin coating for enhancing cell adhesion and osteogenic differentiation. Colloids Surf B Biointerfaces 2018;169:233–41.
[37] Zhao Y, Wong HM, Wang W, Li P, Xu Z, Chong EY, et al. Cytocompatibility, osseointegration, and bioactivity of three-dimensional porous and nanostructured network on polyetheretherketone. Biomaterials 2013;34(37):9264–77.
[38] Zhu Y, Cao Z, Peng Y, Hu L, Guney T, Tang B. Facile surface modification method for synergistically enhancing the biocompatibility and bioactivity of poly(ether ether ketone) that induced osteodifferentiation. ACS Appl Mater Interfaces 2019;11(31):27503–11.
[39] Wu CL, Harasymowicz NS, Klimak MA, Collins KH, Guilak F. The role of macrophages in osteoarthritis and cartilage repair. Osteoarthritis Cartilage 2020;28(5):544–54.
[40] Madry H, Kon E, Condello V, Peretti GM, Steinwachs M, Seil R, et al. Early osteoarthritis of the knee. Knee Surg Sports Traumatol Arthrosc 2016;24(6):1753–62.
[41] Chen Z, Bachhuka A, Han S, Wei F, Lu S, Visalakshan RM, et al. Tuning chemistry and topography of nanoengineered surfaces to manipulate immune response for bone regeneration applications. ACS Nano 2017;11(5):4494–506.
[42] Chen Z, Ni S, Han S, Crawford R, Lu S, Wei F, et al. Nanoporous microstructures mediate osteogenesis by modulating the osteo-immune response of macrophages. Nanoscale 2017;9(2):706–18.
[43] Liu W, Li J, Cheng M, Wang Q, Yeung KWK, Chu PK, et al. Zinc-modified sulfonated polyetheretherketone surface with immunomodulatory function for guiding cell fate and bone regeneration. Adv Sci 2018;5(10):1800749.
[44] Li L, Long J, Li L, Cao H, Tang T, Xi X, et al. Quantitative determination of residual 1,4-dioxane in three-dimensional printed bone scaffold. J Orthop Translat 2018;13:58–67.
[45] Wang Y, Zhang W, Yao Q. Copper-based biomaterials for bone and cartilage tissue engineering. J Orthop Translat 2021;29:60–71.
[46] Deng C, Chang J, Wu C. Bioactive scaffolds for osteochondral regeneration. J Orthop Translat 2019;17:15–25.